Journal of Building Engineering 112 (2025) 113677

Contents lists available at ScienceDirect

Journal of Building Engineering

journal homepage: www.elsevier.com/locate/jobe

Integrated design framework for optimizing shape and Damper placement in steel gridshells under seismic loads

Alireza Hosseini [a], Bruno Briseghella [b], Gian Felice Giaccu [c], Luigi Fenu [a,*]

[a] University of Cagliari, Cagliari, Italy
[b] Fuzhou University, Fuzhou, China
[c] University of Sassari, Sassari, Italy

ARTICLE INFO

Keywords:
Parametric design
Shape optimization
Gridshell
Viscoelastic damper
Seismic performance

ABSTRACT

This paper introduces a design methodology to enhance the seismic response of gridshells by simultaneously optimizing their shapes and the configuration of viscoelastic dampers. While viscoelastic dampers effectively reduce seismic responses, their impact on gridshell geometry has received limited attention. The proposed framework integrates damper placement into the initial design stage to address this gap, unlike conventional approaches that treat geometry and damper design separately. Leveraging parametric geometric and structural modeling, combined with a genetic algorithm, the framework utilizes a multi-phase fitness function derived from static and dynamic analyses, accounting for damping effects and material and geometric nonlinearities. The findings reveal that, as the number of dampers increases, optimized gridshells tend to adopt more elliptical shapes while achieving substantial reductions in both maximum displacement (exceeding 50 % in some cases) and thrust forces (up to 40 %), with the effect being more pronounced in mid-rise domes. Notably, even configurations with as few as 32 dampers can yield satisfactory seismic performance. Overall, locally symmetric damper layouts are recommended. The proposed methodology underscores the benefit of integrating damper placement with shape optimization during the early design phase, enabling adaptable applications to other structural systems and supporting more informed performance-based design decisions.

1. Introduction

The integration of structural considerations into architectural geometry has emerged as one of the most critical research topics, as highlighted by Pottmann and Bentley [1]. Optimizing a structure's shape through structural analysis allows architects and engineers to significantly improve both the aesthetic and functional aspects of a design. This approach becomes particularly important when incorporating damping devices, which can alter a structure's behavior so substantially that the optimal shape may deviate from the initial design. In this context, gridshell domes present an ideal case study due to their parametric design flexibility and fewer constraints, allowing for greater optimization potential.

Gridshell domes, characterized by their geometrically distinct and efficient reticulated structure, have gained prominence in modern architectural design for their remarkable blend, aesthetic elegance, and structural efficiency. These interlocking beams' lattices form a shell-like, curvilinear surface that is both lightweight and robust under gravity loads and can span large areas without

* Corresponding author.
E-mail address: lfenu@unica.it (L. Fenu).

https://doi.org/10.1016/j.jobe.2025.113677
Received 22 April 2025; Received in revised form 11 July 2025; Accepted 2 August 2025
Available online 6 August 2025

internal support [2]. However, due to slender steel members, they have low global stiffness and damping, consequently showing possible instability under dynamic forces, which is an issue in earthquake-prone regions [3,4]. To address this possible drawback, increasing the stiffness by adding layers to the gridshell has been studied by various researchers [5,6], while in other studies, the application of partial double-layer has been proposed [7,8]. On the other hand, the pursuit of enhancing seismic performance has led to the innovation of various vibration control mechanisms. The primary emergence of structural control devices and seismic isolation techniques goes back to the 1970s and 1980s, with the invention of new elastomeric bearings and sliding systems in the 70s and the appearance of active and passive structural control systems in the 80s [9].

Evidencing the effectiveness in energy absorption of vibration control systems [10] and their economic improvement, in the past decades the importance and value growth of the structures, as well as the facilities inside them, encouraged the development of novel utilization of control devices, such as isolators merged with mitigation devices [11]. Consequently, in order to utilize viscoelastic dampers as a cost-effective and reliable solution to mitigate energy, more investigations in optimizing the dampers' properties and the placement and distribution of control devices in buildings are performed by Refs. [11,12]. Yang conducted a study in which selected bars of a double-layer reticulated shell dome were replaced by viscoelastic (VE) dampers, identifying an optimal damper topology [13]. It is observed that while adding dampers typically enhances structural stiffness, replacing structural members with dampers can, conversely, reduce stiffness. Consequently, the selection and specification of dampers play a crucial role in maintaining structural integrity and controlling deformations. In his study, Yang employed VE dampers with linear behavior and fine-tuned them in accordance with the design strategy of replacing structural members with dampers. Zhi investigated the failure modes of single-layer reticulated shells, introducing dynamic instability and strength failure when subjected to dynamic loads [4]. Strength failure with prior warning signs was proposed as an optimized design [14]. To counteract buckling and dynamic instability, it was suggested to increase the dome's rise/span ratio and incorporate a partial double-layer design [15]. For high rise-to-span ratio domes, strengthening the elements in the second ring from the top was also suggested [16].

In structural engineering, the optimization of damper configurations in conventional buildings has been a focus of extensive research [17–23]. The efficacy of optimized viscoelastic (VE) dampers in shock absorption was demonstrated by some researchers [24]. Furthermore, it was found that fewer dampers with higher damping coefficients are more effective than a greater number of dampers with lower coefficients [25]. However, research on gridshell structures typically focuses on examining and selecting the most effective damper configurations from specific options. Zhou et al. [26] employed genetic and gradient-based algorithms to optimize semi-active damper placement in spatial reticulated structures and identified the lower three rings as the most effective location. This was further corroborated by Yang and Ma, who reported that the optimal viscoelastic (VE) damper placement is achieved when dampers replace diagonal bar members in the lowermost three rings of the reticulated shell [27]. Moreover, Yang compared the structural responses of 14 double-layer Kiewitt-8 gridshells featuring various damper placement topologies to identify the optimal topology. An "energy absorption band" by replacing diagonal members with dampers exclusively in the lowest ring was proposed [28]. The proposed dampers' topology incorporated 40 VE dampers in a Kiewitt-8 gridshell, yet it did not explore variations beyond this specific arrangement.

While previous works have addressed related optimization problems, such as minimizing the number of actuators to reduce cross-sectional areas in prestressable truss and cable systems [29], the simultaneous optimization of gridshell shape and damper configuration has not yet been explored. Addressing this gap, the present study introduces a novel design strategy that enhances structural performance by moving beyond the traditional sequential approach—where geometry is defined first, and dampers are added later to improve seismic response. Instead, this methodology simultaneously optimizes the structure's shape and damper configuration, achieving a more integrated and efficient design process.

The study employs parametric modeling to analyze various parameters using advanced optimization techniques comprehensively. The geometric definition of the gridshell is developed in Grasshopper, while structural analysis is conducted using the finite element software OpenSees [30]. The dampers' characteristics are determined based on existing literature, with sensitivity analysis employed to identify optimal damping coefficients and stiffness values. To thoroughly evaluate the structure's seismic response and effectively capture the impact of the seismic dampers, a dynamic analysis is essential. Therefore nonlinear time-history analyses are conducted, encompassing material and geometric nonlinearity. The research advances further by employing an Evolutionary optimization algorithm, specifically a Genetic Algorithm, to refine the VE damper configurations in the lowest ring of gridshell domes. Beyond merely applying the concept of the "energy absorption band", which integrates dampers at the gridshell's first ring, this investigation delves into the optimization of damper configurations alongside shape optimization. It aims to deepen the understanding of how VE damper deployment, influenced by variations in rise-to-span ratio and base tangent inclination, can strengthen seismic performance in gridshells. This exploration yields insights into the optimal arrangements of dampers and their impact on the optimal shape of gridshell domes, improving their seismic performance.

2. Proposed design framework

This study introduces a parametric design framework aimed at simultaneously optimizing the geometric shape and the VE damper configuration of dome structures, particularly under the influences of vertical static and horizontal transient loads. The framework utilizes design variables to parametrically define the dome shape through a cubic Bezier curve, enabling thorough parametric modeling. This structural model undergoes analysis within the OpenSees environment, where the integration of dome geometry and VE damper placement is parametrically defined, ensuring a seamless melding of dampers within the finite element model. The framework takes into account material and geometric nonlinearity and employs both gravity and time-history analyses to assess the structural response to static and dynamic forces. Optimization, conducted through a genetic algorithm, aims for the concurrent

refinement of the dome shape and damper arrangement. The primary objective centers on minimizing the displacement observed in the gridshell dome, with critical constraints including member strength, maximum allowable deformation, and buckling resistance, to ensure the structure's integrity and performance. The study procedure is introduced in Fig. 1.

2.1. Parametric model

To parametrically define the single-layer steel gridshells' geometry, as shown in Fig. 2, this study employs Grasshopper, a visual programming language within Rhino 3D, due to its well-known capability in parametric modeling, enabling greater control over form generation (nodes coordination) and the flexible introduction of the gridshell members (nodes networks).

2.1.1. Parametric definition of the dome shape

Parametric modeling of the dome initiates with the use of a 2D cubic Bezier curve, defined in Eq. (1), to establish its basic shape. Bezier curve is a parametric curve, famous in computer-aided design software that is generated with 'control points' [31]. As shown in Fig. 3, the gridshell dome's geometry is principally determined by two main parameters: the height of the middle control points (P_1 and P_2) and their distance. Nevertheless, these input parameters have a direct correlation with the curve apex height (H) and the curve's slope of tangent (α), thereby using these latter parameters to describe the dome shapes. In contrast to common dome design which is typically characterized by the 'rise' of a circular arc, the Bezier curve's strength is its flexibility; modifying particularly the slope of tangent at the curve's ends, enables the creation of diverse arrays of shapes, including forms similar to catenary, spherical, and ellipsoidal.

$$B(t) = P_0(1-t)^3 + 3P_1t(1-t)^2 + 3P_2t^2(1-t) + P_3t^3 \qquad 0 < t < 1 \tag{1}$$

The 3D shell is configured to conform to the predetermined Bezier curve. The dome is divided into eight radially symmetric sections, following the 'Kiewitt-8' terminology. Its layout consists of six concentric rings formed by latitudinal elements, which are generated by subdividing the Bézier curve into 12 equal segments. This segmentation into symmetrical sectors significantly enhances the efficiency of parametric modeling, allowing for more precise control and uniformity in the structural design of the gridshell dome (Fig. 4).

The gridshell elements are classified into three types: radial, latitudinal, and diagonal (Fig. 4a). The members of each ring are individually defined to allow for specific and distinct attribute assignments. To demonstrate the effectiveness of the proposed methodology, the Kiewitt-8 gridshell dome, with a span of 60 m, was selected for this study. Its member distribution allows for straightforward parametric modeling, making it an ideal candidate for investigation. Furthermore, the availability of previous research [28], applying dampers to this type of gridshell dome, supports the validation of the proposed models. In this case, the model consists of 456 lines connecting 169 nodes to form the Kiewitt-8 gridshell dome. This configuration, while maintaining a fixed node network, allows for the adjustment of nodes' coordinates based on the initial Bezier curve, demonstrating the model's adaptability. In this way, all the grid-shell members are automatically defined.

2.1.2. Parametric definition of the damper configuration

Besides the parameters used to define the gridshell geometry, a further parameter was introduced listing all the possible ways of

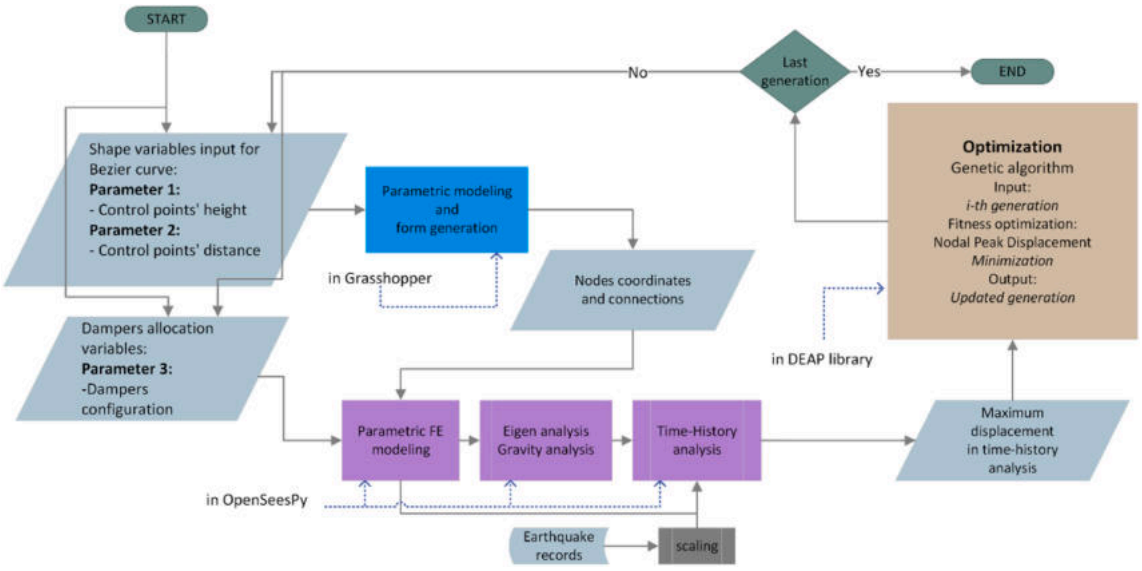

Fig. 1. Study procedure.

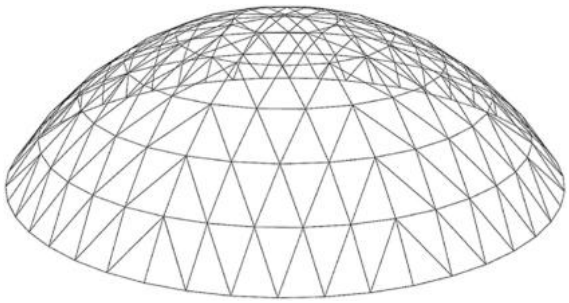

Fig. 2. Kiewitt-8 gridshell dome- 3D view.

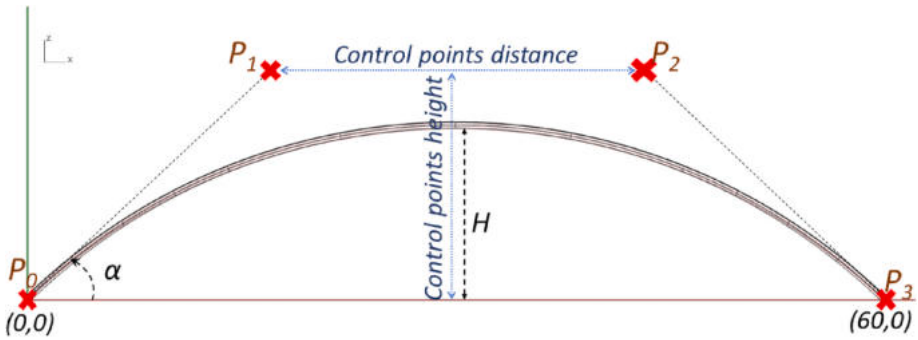

Fig. 3. Initial 2D Bezier curve definition.

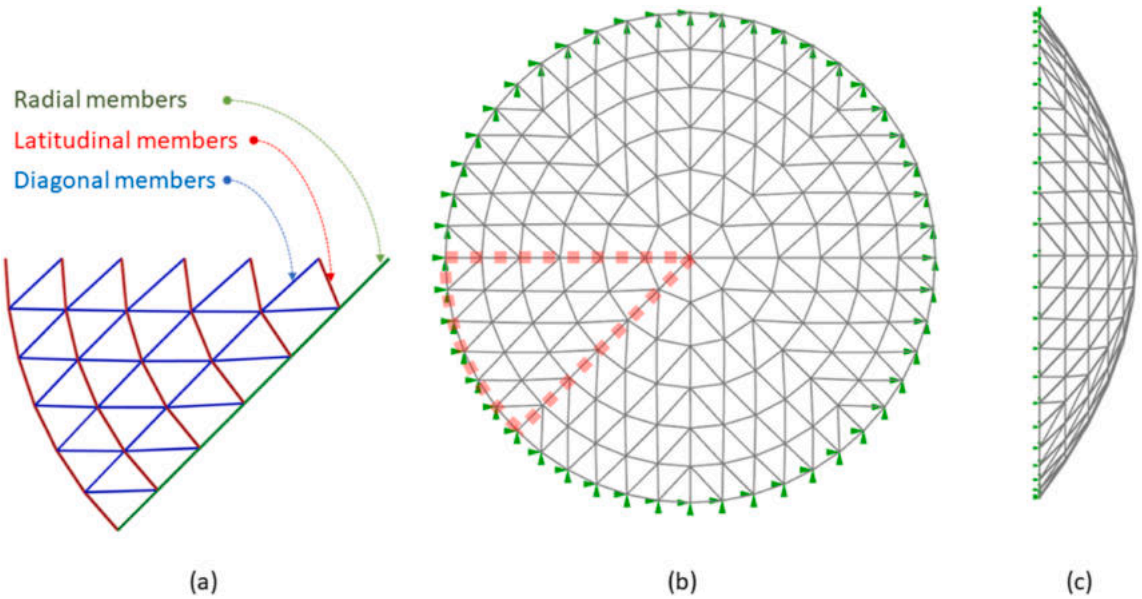

Fig. 4. (a) One-eighth of the Kiewitt-8 dome. (b) Top view of the dome. (c) Side view of the dome.

suitably substituting a number of diagonal members of the gridshell with VE dampers. This last parameter, together with the two parameters of the Bezier curves describing the gridshell shape (univocally related to height and base tangent inclination), are the ones used in the optimization procedure described in Section 4. The diagonal members are suitably replaced by VE dampers only in the first ring of the six concentric rings constituting the Kiewitt-8 gridshell under consideration (see Fig. 4). The dampers' topology is defined only within one-eighth of the dome, as the gridshell is composed of repeated one-eighth segments, ensuring consistent structural

responses to seismic forces from different directions in real-world scenarios. The resulting configuration is then mirrored across the remaining symmetrical sections of the structure (Fig. 4).

Fig. 5 illustrates a one-eighth segment of the Kiewitt-8 gridshell dome's first ring, detailing the numbering of the 10 diagonal members of this segment. Table 1 shows how to represent two damper configurations, one locally symmetrical and the other asymmetrical. The presence or absence of dampers is represented by '0' (indicating damper absence) and by '1' (indicating the replacement of the diagonal member with a VE damper). Note that the total number of possible damper configurations (symmetric and asymmetric) is very high, namely 1024 possible configurations.

It is important to note that displaying all possible damper topologies, comprising 1024 symmetric and asymmetric configurations, is not feasible. However, by assuming only locally symmetrical topologies, as in Opt. 3 (explained in section 4), the number of possible configurations is reduced to 2^5 (or 32), making them more manageable to analyze and present. Fig. 6 shows all 32 locally symmetric damper topologies. To maintain symmetry within individual one-eighth segments, the number of applied dampers must be an even number, namely 2, 4, 6, 8, or 10, that, multiplied by 8 (the number of one-eight gridshell segments), correspond to, respectively, 16, 32, 48, 64, or 80 total number of dampers in the entire locally symmetric gridshell.

The damper configuration cannot be directly represented by a single numerical value; therefore, for clarity, each topology is assigned a unique numerical identifier (ID). This means, for example, that the locally symmetric topology of Table 1 is identified by ID 10 (see Fig. 6), and is in turn handled by the GA algorithm as binary number 0, 1, 0, 1, 0, 0, 1, 0, 1, 0.

Upon generating node coordinates and connections in Grasshopper, the finite element model is constructed in OpenSees (Open System for Earthquake Engineering Simulation) [30], utilizing these coordinates and links (explained in 2.2). The integration of OpenSeesPy [32] facilitates parametric modeling, enabling the exploration of various design scenarios. This capability is particularly advantageous as it allows OpenSees to be combined with optimization algorithms, thereby aiding in identifying optimal design solutions for the structural models under consideration (See Fig. 1).

2.2. Structural model

The single-layer Kiewitt-8 gridshell dome, depicted in Fig. 4a is composed of eight radial members (meridians) arranged symmetrically, with six latitudinal rings evenly dividing the meridians along their length. The diagonal members within each one-eighth segment of the dome are distributed symmetrically, ensuring balanced structural behavior. The structural elements are constructed using steel circular hollow sections, all possessing identical mechanical characteristics, as detailed in Table 2. The material behavior is modeled using the 'steel01' material model in OpenSees, which accounts for uniaxial bilinear response and incorporates kinematic hardening effects. The gridshell employs two distinct member sizes: diagonal members utilize sections of Φ159 × 6.3 mm, while Φ152 × 5.0 mm sections are specified for both radial and latitudinal members, as detailed in Table 3.

In the FE model, all members are rigidly connected. Welded joints are used, and their verification is always satisfied according to the Eurocode 3 rules on CHS (Circular Hollow Section) joints [33–36]. When members are replaced by VE dampers, a hinged connection is used to eliminate bending moments in the VE dampers, ensuring their proper functionality and effectiveness. The structure is fixed by 48 nodes, each featuring three-way hinges. The elements are modeled as inelastic displacement-based frame elements using the 'dispBeamColumn' command in OpenSees, incorporating five integration points along their length and eight fibers across the cross-section to represent the tube bar members (Fig. 7). A design load of 2 kN/m^2 is assumed for the roofing system, evenly distributed among the nodal points. Rayleigh damping ratio of 2 % is applied, which is periodically recalibrated with the updating stiffness matrix. Accordingly, the first two predominant natural frequencies of the system from eigen analysis are used for a_0 and a_1 in Eq. (2) [37].

$$c = a_0\, m + a_1\, k \tag{2}$$

Given that thousands of structural configurations are analyzed, a_0 and a_1 are automatically computed for each case. To provide a reference, the baseline dome with H = 12m and α = 43.5° (tan α = 0.95) has dominant periods of 0.11 s and 0.42 s, yielding a_0 = 0.4717 and a_1 = 0.00055 for 2 % damping.

In this investigation, various rise-to-span (R/S) ratios for the dome are examined. However, an R/S ratio of 1/5, corresponding to a rise of 12 m with a tangent of 43.5°, is chosen as the reference model. This ratio is used for illustrative purposes in figures and sections that focus on a singular dome shape configuration.

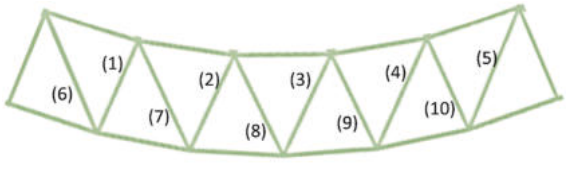

Fig. 5. The first ring of one-eighth of Kiewitt-8 dome with diagonal elements notation.

Table 1
Chromosome representation of a locally symmetric and asymmetric dampers' topology.

Element No.	1	2	3	4	5	6	7	8	9	10	Scheme
Locally Symm. Topol.	0	1	0	1	0	0	1	0	1	0	
Locally Asymm. Topol.	0	0	1	0	1	1	1	1	1	0	

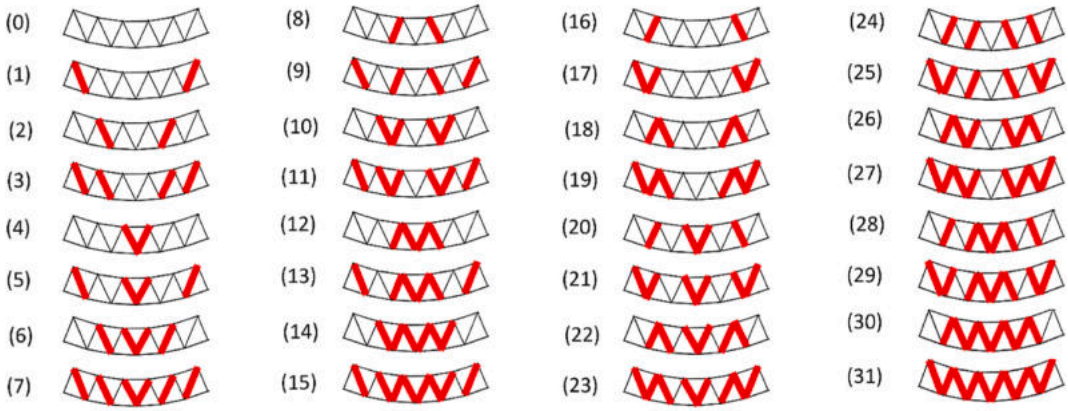

Fig. 6. Locally symmetric topologies of diagonal members of the first ring with VE dampers (red shows dampers).

Table 2
Steel properties.

Mechanical Property	Magnitude
Elastic modulus (E)	206 GPa
Yielding stress (f_y)	235 MPa
Strain-hardening ratio	0.002

Table 3
Members cross-section sizes.

Element type	Diameter x thickness
Latitudinal members (mm)	159 x 6.3
Radial members (mm)	159 x 6.3
Diagonal members (mm)	152 x 5.0

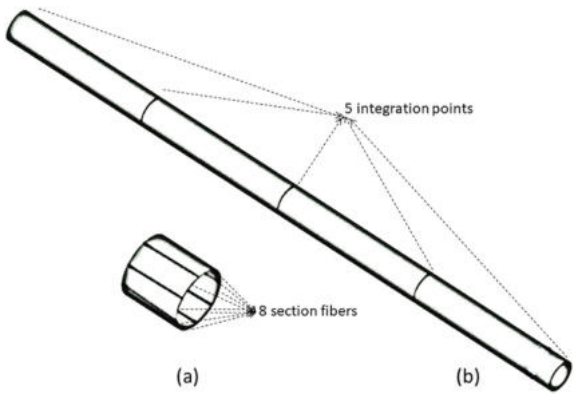

Fig. 7. Members numerical model; (a) Fibers in the cross-section and (b) integration points along elements.

2.3. Viscoelastic Damper

In alignment with the methodologies proposed by previous studies [27,28], this research also implements linear VE dampers as replacements for structural elements. The design of these dampers involves two key parameters: damping, defined by the 'Viscous' material [38], and stiffness, characterized by the 'Elastic' material in OpenSees. The dampers are modeled using the Kelvin-Voigt model, where the damper's stiffness and damping components operate in parallel and are formulated as Eq. (3). It is important to note, as highlighted in the introduction, that while adding dampers into a system enhances its overall stiffness, substituting a steel member with a VE damper reduces the system's total stiffness. Therefore, to mitigate the risk of excessive deformation, particularly under strong seismic excitation where drift control is critical, a linear viscoelastic damper model was adopted. This choice is consistent with the modeling of VE dampers in the literature, where linear Kelvin-Voigt elements are commonly used [13,28]. Additionally, studies have shown that linear fluid viscous dampers can outperform nonlinear ones in drift control under high seismic intensities [39–41], supporting our approach from both modeling and performance perspectives.

$$F = kx(t) + c\dot{x}(t) \tag{3}$$

In the literature, the use of dampers for the seismic protection of gridshells has garnered significant attention from researchers. For example [27] achieved optimal topology using 96 dampers with VE stiffness (K=60 kN/m) and damping coefficient (C_d=100 kN s/m) for double-layer Kiiewitt-8, while Xu et al. [28]used 40 VE dampers with C_d = 500 kNs/m and K_d = 600 kN/m for a single-layer Kiewitt-8 dome with rise-to-span of 1/5. In this study, the VE dampers are assigned parameters of C_d = 700 kNs/m and K_d = 700 kN/m representing relatively small-sized dampers. This is a critical consideration for their practical application in roofing systems. The proposed VE damper properties are constant for all the models; thus, the parameters are selected considering their effect on different configurations of the dome and the dampers. VE dampers are modeled using 'zero-length' elements working uniaxially and added to an 'elasticBeamColumn' element which represents the member that the damper is mounted on as shown in Fig. 8.

Similar to the parametric modeling of the structural members defined in the previous section, the dampers are allocated to one-eighth of the dome and this arrangement is mirrored in its symmetrical sections. This approach potentially increases the damper count by a factor of eight, potentially totaling 80 if each element in the lowest ring would be a damper.

3. Seismic action

To optimize the dome shape and bar-damper configuration, a seismic performance analysis is performed to evaluate the structural responses under significant seismic actions. The adopted methodology primarily incorporates assumptions and performance criteria from Eurocode 8 [42]. To identify ground motions compatible with a performance-based approach, the design earthquake parameters consistent with the EC8 design response spectrum are defined. These parameters are then scaled to fit the design spectrum using the Spectral Matching approach [43,44] as well as the time domain spectral matching method which is developed by Ref. [45] and adopted in SeismoMatch [46].

The set of seven selected earthquake records is described in Table 4 and shown in Fig. 9. This study considers the main horizontal component of the records. Although the vertical component can influence shell structures in specific cases, particularly in shallow configurations, the aim of this paper is to introduce a novel methodology for the optimal seismic design of grid-shell structures equipped with dampers. To streamline the presentation of the approach, the case study neglects the vertical seismic component, a simplification also adopted in Ref. [47]. It should be noted, however, that the proposed methodology has been validated in studies incorporating vertical excitation [28]. These validations confirm that the horizontal component remains predominant, supporting the general applicability of the approach. Thus, the seismic analysis of the structure is performed under one-directional excitation, as the axisymmetry of the gridshell makes the structural response largely insensitive to the direction of horizontal ground motion. The average misfit in the accelerogram matching of the selected ground motions is 3.6 %, and the maximum ground acceleration of the accelerogram's mean is 0.95g—illustrated in Fig. 10.

4. Structural analysis and optimization procedure

With the finite element (FE) model established, the analysis begins with an eigenvalue assessment to determine the modal

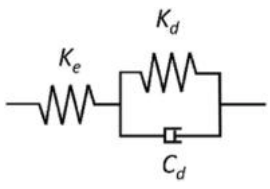

Fig. 8. Schematic representation of a structural member with an applied VE damper, illustrating the member's equivalent stiffness (K_e) and the VE damper's stiffness (K_d) and damping coefficient (C_d).

Table 4
Earthquake records descriptions.

Event	Year	Magnitude Mw	$V_{s,30}$ (m/s)	Record Station	Predominant period (sec)
Corinth	1981	6.6	361	Corinth	0.34
Landers	1992	7.28	379	Joshua Tree	0.48
New Zealand-02	1987	6.6	551	Matahina Dam	0.36
Manjil	1990	7.37	724	Abbar	0.50
Hector	1999	7.13	726	Hector	0.50
Imperial Valley-02	1940	6.95	213	El Centro	0.56
Northridge	1994	6.69	402	Sunland	0.38

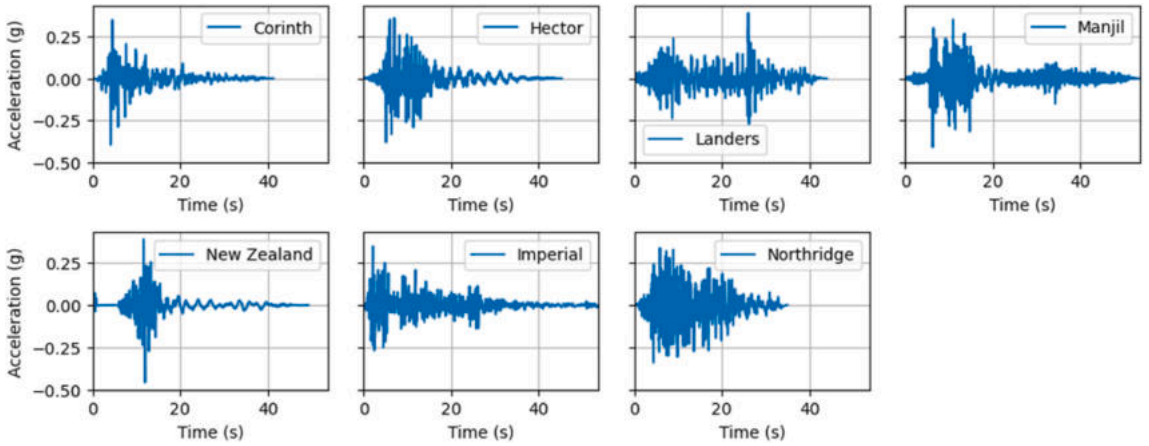

Fig. 9. Accelerograms

Further site-specific assumptions categorize the ground type as Type B, an importance factor of III, and a reference peak ground acceleration (ag_R) of 0.25g.

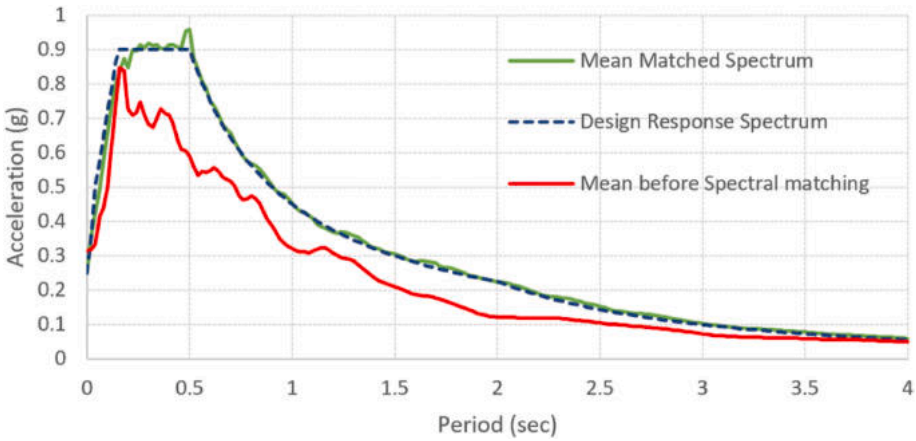

Fig. 10. Mean spectrum of the records before and after spectral matching.

characteristics of the dome structure, including mode shapes and natural periods. The frequencies of the first two dominant modes are used to define the Rayleigh damping parameters, as described in Eq. (1). A static analysis is then conducted to account for gravitational forces, including the self-weight of the structure and imposed design loads. Following this, a dynamic time-history analysis is performed on the deformed model obtained from the static analysis results. This dynamic analysis incrementally applies seismic accelerations derived from the selected earthquake record data to evaluate the structure's response. This study incorporates both geometric and material nonlinearities, as members may exceed the yielding criteria, particularly in uncontrolled systems (i.e. without seismic dampers). Additionally, geometric nonlinearity is crucial for controlling buckling phenomena.

To assess the seismic performance of the damper's configurations, generated by an optimization routine, the study tracks the

displacement at the dome's highest point and the maximum nodal displacement. The displacement at the highest point is indicative of the overall structural deformation, whereas the maximum nodal displacement provides critical insight into localized deformations, which, according to existing studies, may not occur at the highest point due to the diversity of modal shapes. Moreover, due to the oblique arrangement of the dome's members, the predominant displacement under lateral seismic forces is not restricted to the horizontal plane. Instead, it may also present in the vertical direction, depending upon multiple factors, such as the dome's rise-to-span ratio and the cross-sectional properties of the structural members. Therefore, this study takes into account the resultant displacement of the X, Y, and Z directions to thoroughly evaluate the dome's response to seismic events. Notably, this maximal displacement is utilized as the key fitness value in the optimization algorithm, offering valuable insight into the structural optimization process.

Additionally, given that the dampers are installed within the lowest ring, their configuration can have a substantial impact on the reaction forces at the dome's base fixed nodes. Consequently, this study records and analyzes the horizontal reaction forces at these support nodes, recognizing their effect on the dome foundation.

In seismic performance optimization, metaheuristic algorithms are often favored due to the complexity of structural systems. The choice of algorithm depends on the specific problem. For instance, single-solution algorithms like *Simulated Annealing (SA)* are effective in avoiding local minima but may struggle with large, complex design spaces where parallel exploration is necessary [48]. *Particle Swarm Optimization (PSO)*, typically used for continuous problems, can be adapted for discrete cases but requires additional mechanisms to handle binary decisions [48].

In contrast, *Genetic Algorithms (GA)* [49] naturally support both discrete and binary variables. In this study, GA's chromosome structure efficiently encodes discrete shape variables and binary damper decisions, offering a streamlined solution for the mixed-variable problem. Its population-based approach allows for broad exploration of the solution space, effectively finding globally optimal solutions while avoiding local minima. Additionally, GA's robustness in handling non-smooth, highly nonlinear objective functions makes it particularly suitable for seismic performance optimization [48].

Given these advantages, GA was selected for its flexibility and effectiveness in addressing the unique challenges of optimizing both shape and damper configurations in gridshell domes.

Structural optimization herein performed consists of:

- Optimization objective: Examining the seismic performance of the structure, the minimization of maximum nodal displacement of all nodes at each time instant ($U(t)$ in Eq. (4)) under different records is defined as the optimization objective.

$$U(t) = \max_{j=1,2,..,169} \sqrt{U_{j,x}(t)^2 + U_{j,y}(t)^2 + U_{j,z}(t)^2} \tag{4}$$

Where j denotes the jth node.

- Optimization variables: The optimization variables are defined in two sections: 1. Defines the shape of the dome by two variables: Bezier curve internal

control points' height (h, parameter 1) with a range of 13–27 m, and secondly the distance between the internal control points (d, parameter 2) that is in the range of 11.5–21.5 m there is also a limit threshold that does not allow the distance between the two control points and their height becomes larger than 10. The correlation between these two optimization variables and H and α are defined in section 2.1.1. The other optimization variable is related to the dampers' configuration (D, parameter 3), where it comes in a set of binary elements in a list with a length of 10 that is derived from 10 diagonal members (Eq. (5)) in the lowest ring of one-eighth of the Kiewitt-8 gridshell dome, explained in section 2.1.2.

$$D_i \in \{0, 1\} \quad for \ i = 1, 2, \ldots, 10 \tag{5}$$

Where $D_i = 1$ represents damper presence and $D_i = 0$ for the absence of the damper.

- Constraints: The mathematical constraints of the optimization procedure are expressed in terms of maximum deflection, maximum displacement, allowable stress, and overall stability. The maximum deflection is constrained to span/200, measured under static gravitational loading. The maximum displacement of the dome is constrained to span/300, measured during time-history analysis. These constraint limits are taken from Eurocode recommendations. The stress in the members is an implicit constraint that is considered by the nonlinear behavior of the materials. Instability may occur due to many reasons, and in this study, it is taken into account by using the P-Delta effect in the geometrical transformation of the members. Accordingly, the optimization algorithm evaluates each shape and damper configuration generated by the genetic algorithm; if a solution exhibits instability or violates material stress limits during nonlinear analysis, it is automatically rejected and excluded from further consideration.

Now, with $U(t)$ defined to represent the maximum displacement among all nodes at each time step, the mathematical optimization problem can be formulated as follows.

$$\underset{h,d,D_i}{\text{minimize}} \quad U(h,d,D)$$

Subject to:

$$13 \le h \le 27$$
$$11.5 \le d \le 21.5$$
$$|h-d| \le 10$$
$$D_i \in \{0,1\}, \qquad i = 1,2,\dots,10$$
$$Deflection\_static_{max} \le {}^{span}/_{200}$$
$$Displacement\_dynamic_{max} \le {}^{span}/_{300}$$
$$\sigma(x) \le \sigma_{allowable}$$
$$stability\ control\ by\ P-\Delta\ convergence$$

Taking advantage of OpenSeesPy for parametric analysis, this study utilized the DEAP (Distributed Evolutionary Algorithms in Python) [50] library to execute a comprehensive optimization through a GA (the flowchart is shown in Fig. 11) across three distinct scenarios.

1. **Dome Shape Optimization (opt. 1):** The first optimization scenario is controlling the height and slope of the tangent of the dome, without the inclusion of any damping devices. In this scenario (opt.1), variable parameter 1 (height of the control points) and variable parameter 2 (distance between the control points) are optimization variables. The objective function is as mentioned.
2. **Damper Configuration Optimization with Fixed Height: (opt.2)** For constant dome height, the focus shifted to optimizing damper placement. Variable parameter 3, which is a binary list of length 10, is adopted to allocate the dampers as a substitute for diagonal elements. This configuration is symmetrically replicated across the other eight sections of the structure. The GA assessed combinations of dampers (indicated by '1's in the binary list) to ascertain those most effective in minimizing the dome's maximum displacement, representing the objective function.
3. **Combined Optimization of Dome Shape and Damper Configuration:** In the final optimization phase, dome shape parameters (variables 1 and 2) were combined with damper configurations (variable 3).

Two scenarios were explored.

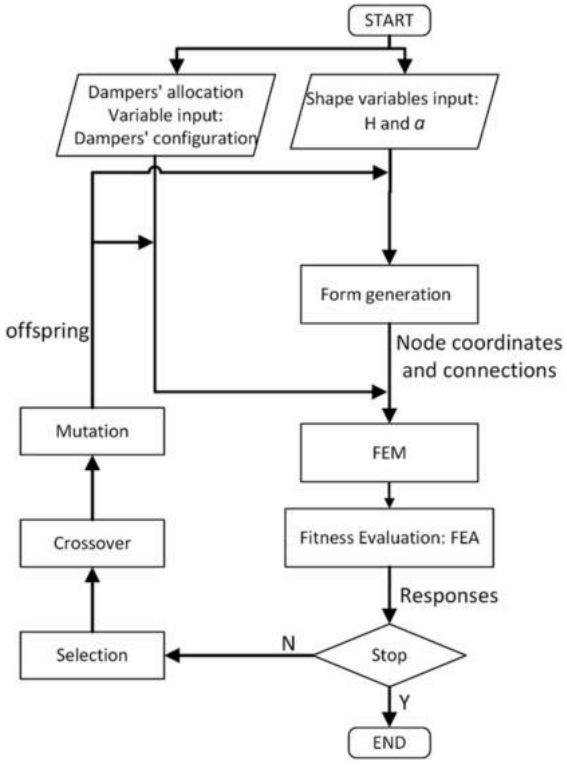

Fig. 11. The general framework of the Genetic Algorithm (GA) used in this study.

- In the first scenario **(opt.3a)**, the variable count was reduced to 7, namely variables 1 and 2, plus 5 damper configurations for variable 3 to create locally symmetrical damper topologies. Note that in locally symmetrical VE damper topologies, the configuration for elements 1 to 5 is mirrored for elements 6 to 10, thus reducing the number of variables from 10 to 5 and ensuring symmetry across the topology. The reduction from 10 to 5 in the number of topology variables allowed by symmetry, as well as from 1024 to 32 in the range of possible topologies, aimed to shorten analysis time and provide clearer result demonstration. These symmetrical topologies defined on one-eighth of the gridshell were then replicated throughout the dome to define the whole damper system.
- In the second scenario **(opt.3b)**, allowing for locally asymmetric topologies, the total number of variables increased to 12 (variables 1 and 2, plus 10 damper configurations for variable 3). This final step encompassed all potential dome shapes and damper configurations. This comprehensive approach provided insights into how the implementation of seismic dampers affects both the optimal dome shape and the ideal configuration of dampers.

The DEAP library provides a flexible platform for developing custom optimization algorithms. Since this study employs two distinct types of individuals—one binary and the other a list. The DEAP library's ability to customize optimization algorithms allows for tailored GA functionalities specific to each type of individual, ensuring efficient and accurate optimization processes. The GA explored various configurations through iterative selection, crossover, and mutation processes, methodically converging toward optimal solutions. The population size was set to 40 for scenarios involving two parameters (height and tangent) and increased to 100 for more complex damper topology optimizations. Selection of the best individual is performed using the attribute 'selTournament' of the DEAP Library of Python. The crossover rates are presented in Table 5, employing the 'cxTwoPoint' attribute for two-point crossover to cut the parent strings in two places before rearranging them with both keeping the original length. The mutation rates are shown in Table 5, with 'mutFlipBit' attribute for the binary inputs of the damper topologies (indpb = 0.35) and 'mutGaussian' attribute for discrete inputs as H and α (indpb = 0.35). The DEAP library's capability to handle diverse data types (floats for height and tangents, binary for damper configurations) was essential in this multifaceted optimization endeavor. Additionally, the adoption of a version of the non-revisiting GA approach further enhanced the efficiency of the GA algorithm by minimizing redundant computations.

5. Results

As previously discussed, this study explores three discrete optimization strategies to enhance the seismic performance of the Kiewitt-8 gridshell, focusing on.

- effect of the variation of the height (H) and the base tangent inclination (α) on the seismic response of the Kiewitt dome;
- effect of substituting some of the braces on the lowest ring of the dome with VE dampers;
- effect of contemporary optimization of height, base tangent inclination, and damper configuration.

Combining the results of these three analyses facilitates a comprehensive understanding of how the insertion of VE dampers influences the Kiewitt-8 dome's optimal shape. The proposed methodology firstly plans to assess the seismic behavior of the gridshell without control devices across various heights (H) and base tangent inclinations (α). Subsequently, the exclusive impact of implementing VE dampers on a constant dome geometry is analyzed to demonstrate the dampers' contribution to seismic performance. Finally, an integrated optimization of height, base tangent inclination, and damper configuration is conducted. This approach facilitates a direct comparison between the optimal configurations of the dome with and without control measures, allowing for a nuanced understanding of the benefits conferred by VE dampers.

Sensitivity analysis revealed that while the stiffness of the dampers does not directly influence their effectiveness, it does affect the overall structural stiffness, which in turn impacts the first mode period. This adjustment can lead to a decrease in maximum displacements by moving away from the seismic record's predominant period—a phenomenon further examined in sections 5.2 and 5.3. Excessively stiff dampers, however, pose a risk of causing divergence in nonlinear time-history analyses.

5.1. Effect of the variation of height and base tangent inclination (opt. 1)

In optimization scenario 1 (opt. 1), the structural response of the Kiewitt-8 lattice dome under seven seismic excitations is studied without the inclusion of any damping devices. The analysis focuses on two geometrical parameters: the control points' reciprocal

Table 5
GA parameters for different optimization scenarios.

Parameter	opt.1	opt.2	opt.3a	opt.3b
No. shape var.	2	0	2	2
No. damper allocation var.	0	10	5	10
No. of chromosomes	428	1024	13696	80896
Population size	40	40	80	150
Crossover rate	0.75	0.75	0.85	0.85
Mutation rate	0.5	0.5	0.5	0.5

distance and their identical elevation, as described in Fig. 3 and Table 6. However, as mentioned before, in the Figures and Tables illustrating the results, these two parameters are transformed into two other variables, the height of the dome and the angle at its base, as they are more intuitive. To allow for a consistent comparison of computational effort, the duration of each optimization scenario is also reported; in this case, the optimization required approximately 375 min.

Fig. 12 illustrates how variations in dome height, resulting from shape optimization using two geometric parameters, affect the maximum displacement of the uncontrolled model across all seven earthquake records. Given the variability in the data and the fact that results are not uniformly available across the full height spectrum, sometimes with only a single, non-optimal configuration per height, the plotted minimum values per 1.5 m height bin are used instead of pointwise minima. This binning approach avoids erratic fluctuations caused by sparse or uneven data and provides a clearer and more representative view of general trends.

As shown in Fig. 13, while top-node displacement exhibits a strong and relatively linear dependence on dome height—resulting in a variation of approximately 60 %—the maximum displacement displays a markedly smaller variation (≈15 %). This difference arises from the fact that maximum displacement is not necessarily governed by the first mode and may occur at any location on the structure, making it more sensitive to localized dynamic effects and contributions from higher modes.

To isolate the effect of base tangent inclination from dome height, the parameter "base angle deviation from arc" is introduced. This allows the influence of α to be evaluated independently of H. In a 2D representation, for any given dome height and span, there exists a unique circular arc that passes through the two base points and the dome apex. As illustrated in Fig. 14, this arc lies geometrically between typical catenary and ellipsoidal profiles with the same rise-to-span ratio. The α parameter is defined as the angular difference between the base inclination of a given dome shape and that of this reference arc. This reference is used because it offers a geometrically consistent midpoint between the two extremes of structural form (flat vs. steep), enabling a systematic comparison of base angles across shapes.

By introducing the shape parameter of base angle deviation from the corresponding arc, Fig. 15 illustrates the relationship between displacement and this parameter for the uncontrolled Kiewitt-8 domes under Corinth earthquake. In this figure, the raw data are shown alongside trendlines for both maximum displacement and top-node displacement, highlighting the response of individual configurations to a specific seismic input. To provide a broader perspective, Fig. 16 presents the aggregated trend across all seven earthquake records, revealing a consistent relationship between base angle deviation and displacement. The trendline indicates that the minimum displacement is typically achieved at a base angle approximately 5° below that of the corresponding arc, suggesting that slightly funicular geometries are generally more effective in reducing seismic response.

While Fig. 15 offers insights tied to a single ground motion, Fig. 16 extends the findings to a wider range of seismic inputs. Together, the two figures demonstrate that both excessively flattened (i.e., strongly negative deviations) and steepened (i.e., positive deviations) geometries tend to increase displacement, particularly in terms of maximum values. In contrast, the top-node displacement is shown to be less sensitive to such geometric variations.

The modal analysis of the gridshell model identifies two dominant mass-participating periods (Fig. 17), showing that depending on different heights and base tangent inclination, one of these two periods becomes the leading period, and duly, the mode shape varies. Shallower domes generally exhibit the dominant mode with a lower period—in the range of 0.10–0.12 s—and the second most dominant mode with a higher period—in the range of 0.40–0.45 s, while more elevated domes tend to have the most dominant mode in the range of 0.40–0.45 s and the secondary dominant mode in the range of 0.10–0.12. s. Fig. 17 provides examples of these two shape modes identified in the H = 12 m model: the lower-period mode concentrates deformation at the lower levels, while the higher-period mode induces displacement in the upper regions of the dome. Fig. 18 illustrates how these modal periods vary across different dome geometries. The maximum displacement obtained from the time-history analysis occurs in the vertical direction in the higher levels of the Kiewitt-8 gridshell (3rd and 4th rings from the ground), thus affirming the modal analysis.

5.2. *Optimum dampers' configuration for given gridshell shape (opt. 2)*

Following the work of Xu et al. [28], which replaced the diagonal elements of the first ring in the spherical Kiewitt-8 gridshell dome with viscoelastic (VE) dampers, this section seeks to optimize the VE damper configuration to explore potentially more effective topologies while also assessing whether Xu et al. [28]'s proposed arrangement remains the most efficient. Furthermore, this section validates the models used in this study by comparing the results with those obtained by Xu et al. [28].

In optimization scenario 2 (opt. 2), the focus is solely on optimizing the damper topology, without considering variations in the dome's shape parameters. A representative shape is selected for this purpose, and the damper topology optimization is applied to that fixed geometry. Specifically, a Kiewitt-8 gridshell dome with an H of 12 m and an α of 43.5° (tan α = 0.95) is used as the base configuration. The optimization details are summarized in Table 7. The optimization process in this scenario required approximately 1254 min.

Performing the optimization process, the fitness values were categorized based on the number of applied dampers. Fig. 19 illustrates the best outcome—minimum peak resultant displacement—achieved for each specific number of VE dampers. To simplify

Table 6
Optimization information of opt. 1.

Variable input parameters	Range of variation	Optimization objective
Height (Control points' elevation)	9.75–20.25 m (13–27 m)	Minimize peak resultant displacement
Base tangent inclination (Control points' distance)	35–70° (11.5–21.5 m)	

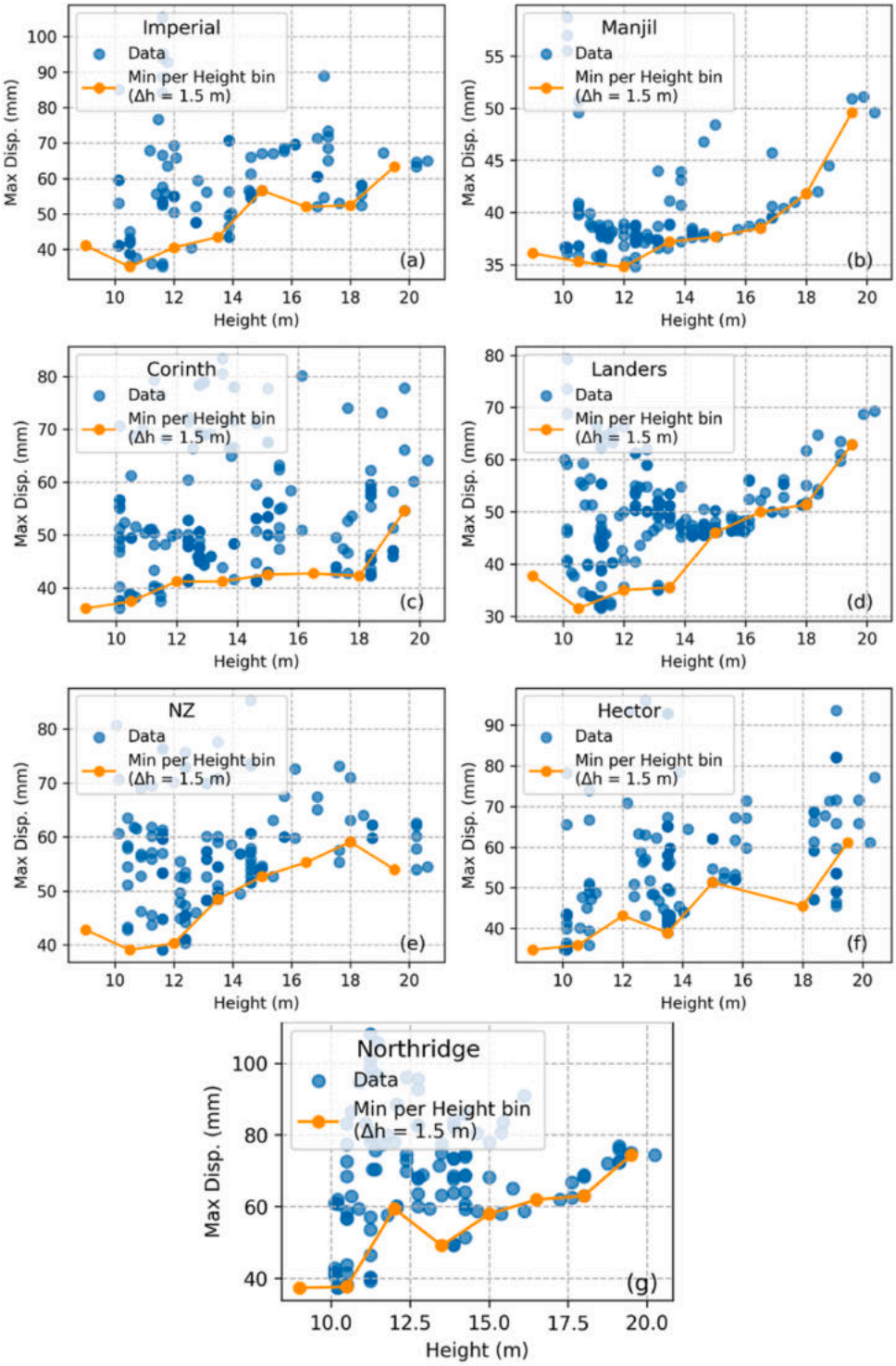

Fig. 12. Maximum displacement of the uncontrolled model plotted against structure height, along with trendlines representing the minimum peak displacement per 1.5 m height bin.

interpretation, this figure highlights the optimal results for each case, showing how different quantities of VE dampers influence the structural performance. The analysis reveals that the optimal number of dampers lies between 32 and 48, where the majority of seismic records exhibit the lowest displacement. Beyond 48 dampers, maximum displacement begins to increase again, suggesting that removing too many structural elements leads to increased deformation that cannot be effectively mitigated, even with additional VE

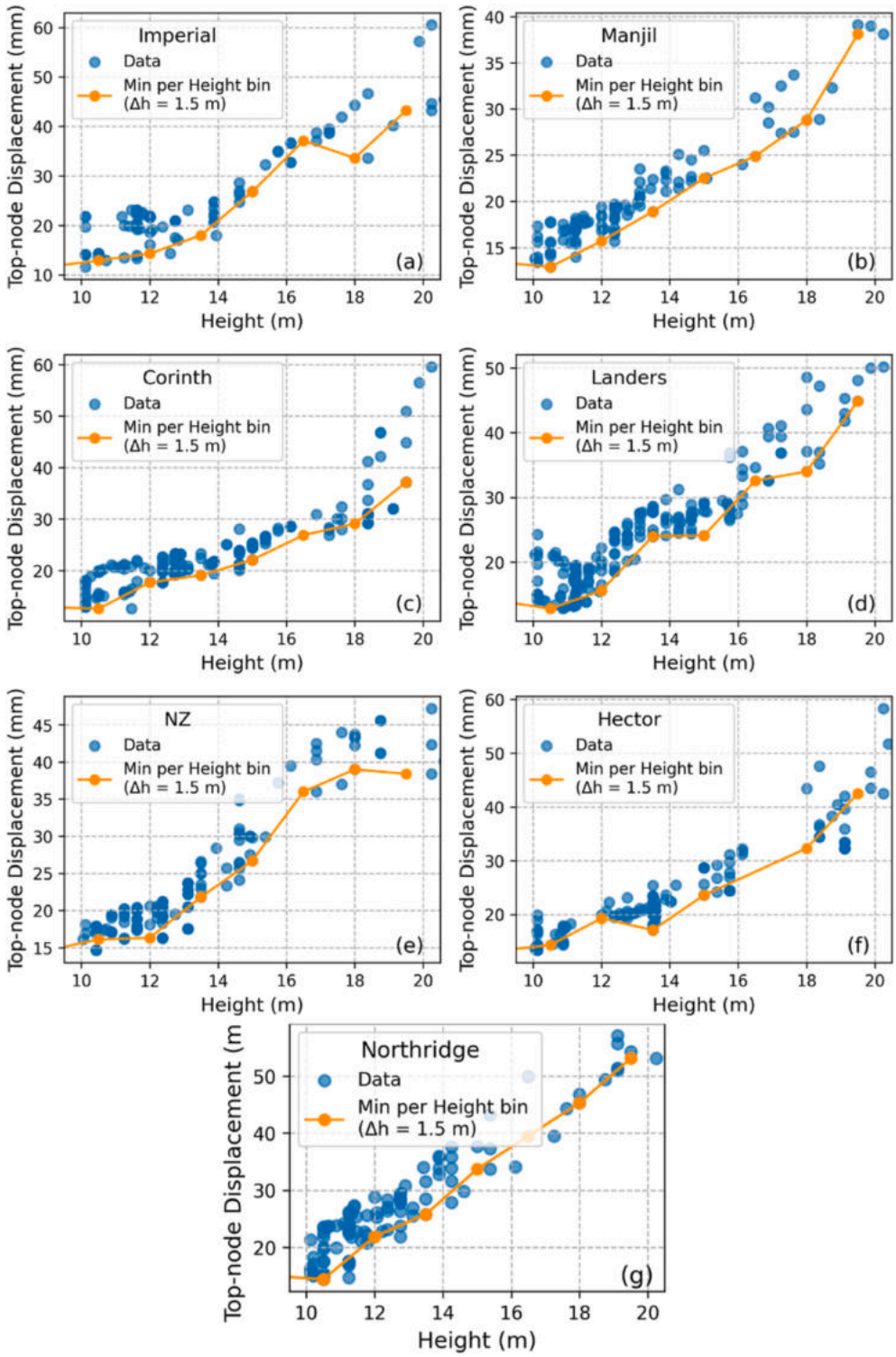

Fig. 13. Maximum top-node displacement of the uncontrolled model plotted against structure height, along with trendlines representing the minimum top-node displacement per 1.5 m height bin.

dampers.

Building on the aforementioned results, which demonstrated optimal performance with 32–48 dampers, this study presents and analyzes specific configurations that minimize structural displacement. The analysis of results presented in Fig. 19 reveals that the

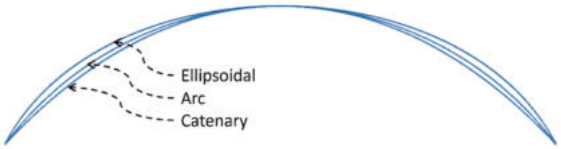

Fig. 14. Geometric comparison of dome profiles with equal rise and span. The circular arc serves as a reference curve positioned between ellipsoidal and catenary shapes, illustrating variations in base angle for the same rise-to-span ratio.

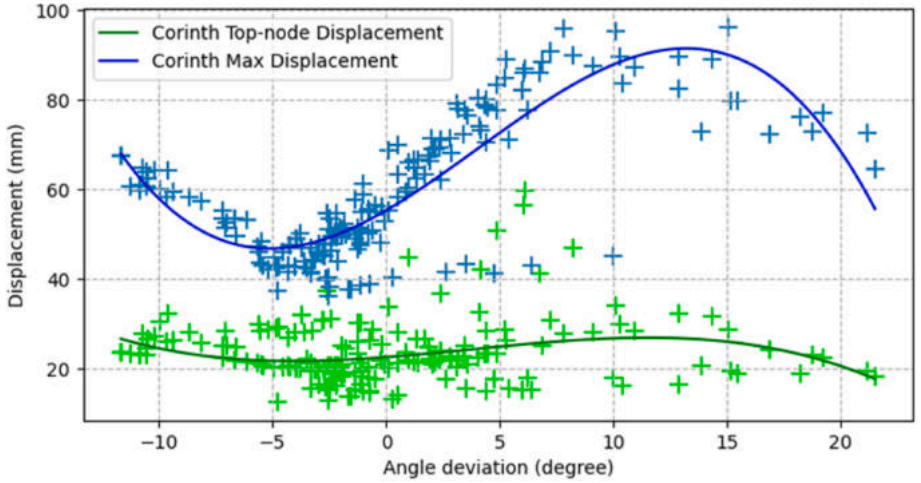

Fig. 15. Raw displacement data and trendline for the uncontrolled model under the Corinth earthquake, plotted against base angle deviation from arc.

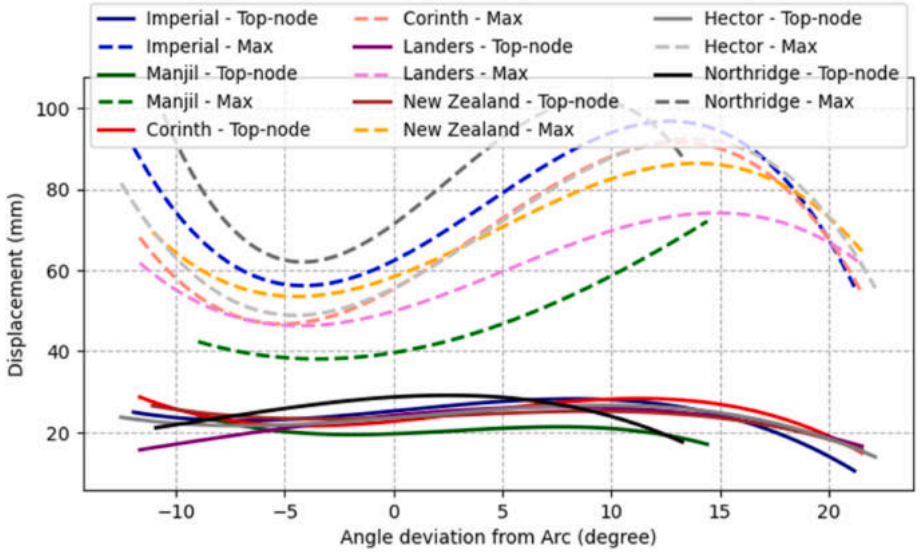

Fig. 16. Overall trend between base angle deviation from arc and displacement for the uncontrolled Kiewitt-8 model, showing the optimal angle range across all records.

optimal topology for minimizing peak displacement in the gridshell varies across different earthquake records. Multiple damper configurations, varying in both quantity and arrangement of VE devices, demonstrated favorable performance under different seismic conditions. This finding suggests that the effectiveness of a particular damper topology is specific to the characteristics of individual earthquake events rather than universally optimal across all seismic scenarios.

To identify configurations that perform robustly across all seismic records, a two-stage decision-making process was implemented.

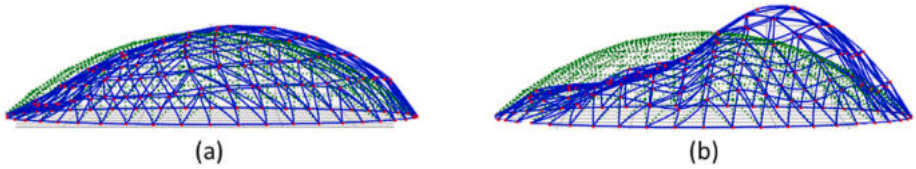

Fig. 17. (a) Shape mode associated with the lower period (T = 0.12 s) and (b) shape mode associated with the higher period (T = 0.41 s) shown for the spherical Kiewitt-8 dome with L = 60 m, H = 12 m, and α = 43.5°. Undeformed shape is shown in green.

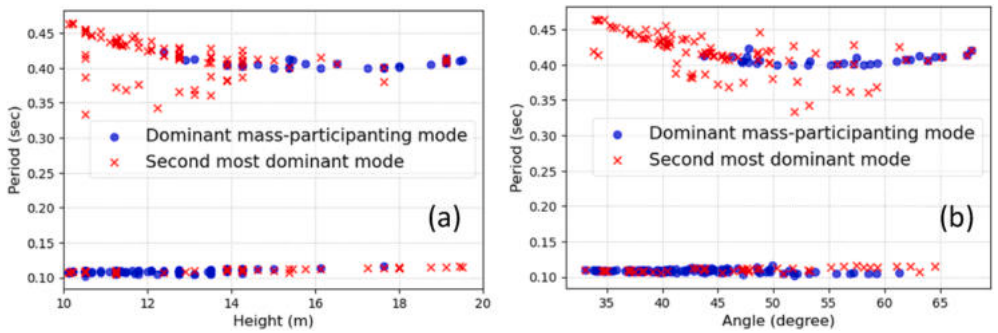

Fig. 18. Variation of the first two dominant mass-participating periods with (a) dome height and (b) base angle, highlighting modal transitions across geometries.

Table 7
Optimization information of opt. 2.

Variable input parameters	Range of variation	Optimization objective
Dampers' Configuration (Topology)	0–1023	Minimize peak resultant displacement

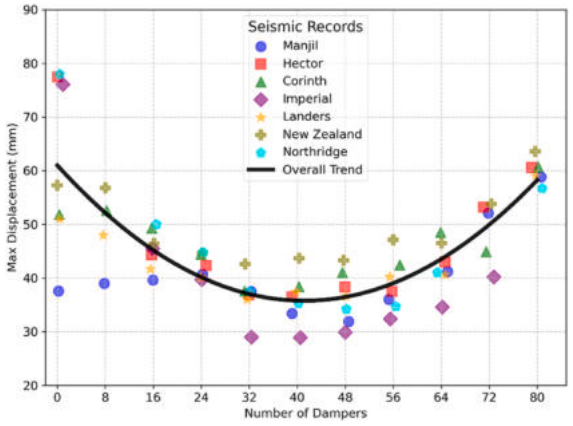

Fig. 19. Maximum displacement for the best topology for each possible number of applied devices under various records.

First, the most effective topologies for each individual earthquake record were identified. These configurations were then comparatively analyzed to determine their overall effectiveness across the complete set of seismic records. This systematic evaluation yielded a ranked list of top-performing configurations, differentiated by marginal variations in their displacement reduction capabilities.

For the comparative analysis, four optimal topologies were selected, each corresponding to a specific damper quantity (representing the most optimal topology for each damper number), as shown in Fig. 20. These topologies, labeled T1 through T4, comprise two locally symmetric and two locally asymmetric layouts: T1 (32 dampers, locally symmetric), T2 (40 dampers, locally asymmetric), T3 (48 dampers, locally symmetric), and T4 (56 dampers, locally asymmetric). While all configurations maintain global symmetry across the entire dome, the locally symmetric layouts (T1 and T3) exhibit additional symmetry within each one-eighth sector of the dome structure.

Fig. 21 effectively demonstrates the considerable benefits of incorporating dampers into the Kiewitt-8 gridshell structure, reducing the dome's maximum displacement. The most significant reductions in maximum displacement—ranging from 40 % to 50 %—are

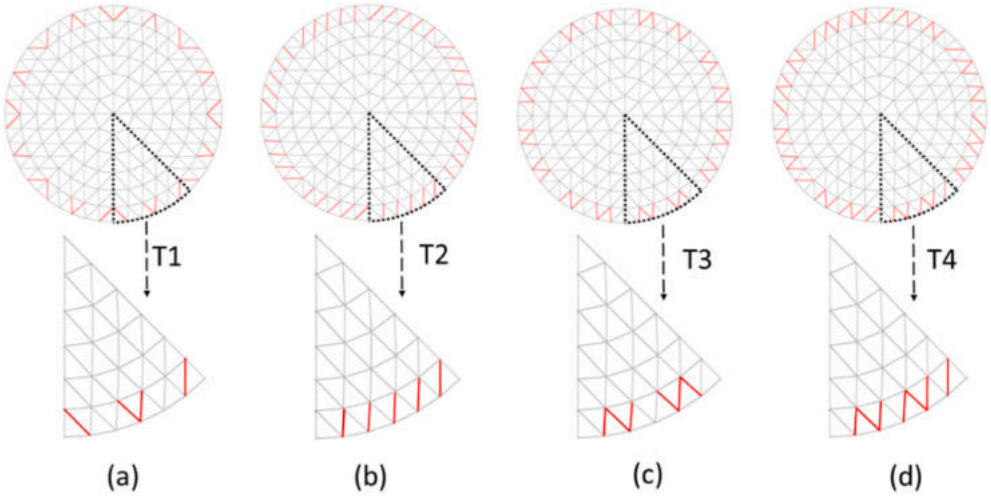

Fig. 20. Dampers' topologies (a) T1, 32 VED, (b) T2, 40 VED, (c) T3, 48 VED, (d) T4, 56 VED.

notably observed in configurations subjected to the Hector, Imperial, and Northridge records, which have the highest maximum displacement in the uncontrolled model. Conversely, for the uncontrolled model exhibiting lower seismic responses to earthquakes like Manjil, achieving displacement reduction through dampers proves challenging across all topologies. In general, all the topologies exhibited similar effectiveness as shown in Table 8, which is important considering the number of applied VE dampers.

In the context of these optimal models, both locally symmetric and asymmetric topologies demonstrate cohesive responses. Among the optimal candidates, the locally asymmetric topology T2 failed to converge under the New Zealand record, due to extensive deformation, which leads to instability of the two adjacent braces in the lower rings. All other topologies and ground motions successfully completed the time-history analysis. Notably, all models, with T3 being a particular example, illustrate their capacity to consistently mitigate maximum displacement to a specific range, independent of the performance of the uncontrolled model. This uniform reduction capability highlights the dampers' effectiveness more distinctly when the uncontrolled model exhibits significantly higher deformation, underscoring the value of damper integration in enhancing structural performance during seismic events.

With regard to the displacement at the dome's top, which reflects the overall behavior of the dome, a maximum reduction of 35 % is observed for configuration T2. This reduction is derived from the average results across all seven earthquake records (see Table 8). However, the dampers have a wider range of effectiveness within different topologies compared to the maximum displacement parameter, with topology T3 achieving an average reduction of 9 %. Notably, the implementation of VE dampers in locally asymmetric configurations demonstrates a more substantial impact than in those that are locally symmetric, as illustrated in Fig. 22.

5.3. Optimization of height, base tangent inclination, and dampers configuration (opt. 3a and opt. 3b)

To conclusively evaluate the effect of VE damper implementation on the dome's optimal shape, optimization Scenarios 3a and 3b

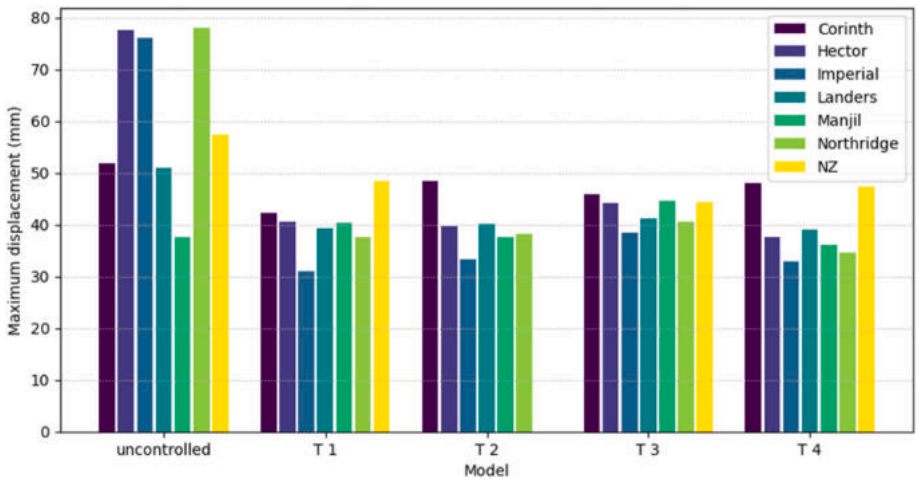

Fig. 21. Comparison of maximum displacement for uncontrolled models and 4 models with applied dampers.

Table 8
Average response reduction of optimal selection topologies compared to uncontrolled model.

	T 1	T 2	T 3	T 4
Maximum displacement	30 %	31 %	25 %	31 %
Top node displacement	14 %	35 %	9 %	25 %

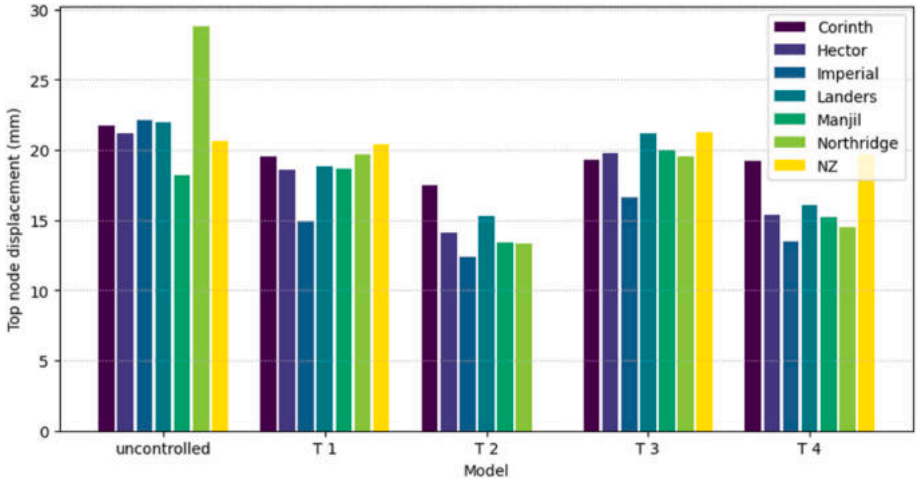

Fig. 22. Comparison of top node displacement for uncontrolled model and 4 models with applied dampers.

(opt. 3a, opt.3. b) consider the simultaneous variation of height, base tangent inclination, and damper configurations are utilized to minimize the Kiewitt-8 gridshell dome's maximum displacement, as detailed in Tables 9 and 11. As outlined in Section 2.1.2, the initial optimization (opt. 3a) focuses on symmetric damper layouts (32 configurations, see Table 9). The procedure is then expanded to include all possible damper configurations—both locally symmetric and asymmetric topologies (totaling 1024 layouts, see Table 11). By structuring the optimization in this way, the first phase offers clear, readable outputs, while the latter part provides a comprehensive evaluation of the damper's impact on the dome's seismic performance and structural optimization. The optimization process for the symmetric configurations alone required approximately 3821 min.

By initially focusing on locally symmetric damper topologies, Fig. 23 illustrates the effect of height variation on the maximum displacement of the controlled gridshell. Although the optimal application of dampers significantly reduces the maximum displacement of the gridshell dome, Fig. 23 shows that, across all seven seismic records, the optimized maximum displacement of the controlled models varies only slightly with dome height. This contrasts with the clear trend observed in the uncontrolled models (see Fig. 12), where lower heights consistently correspond to reduced displacements. In the controlled cases, as illustrated by the orange trendlines in Fig. 23, the influence of height on overall maximum displacement appears marginal, likely due to the combined effect of damping and modal shifts across configurations. However, when focusing on the top-node displacement, Fig. 24 reveals a more pronounced sensitivity to height variation: reducing the dome height leads to a significant decrease—an average of 43 %—in top-node displacement. This suggests that, while the global maximum displacement becomes less height-dependent with damper implementation, the top-node motion remains strongly influenced by geometric parameters. This is because the top-node displacement is governed primarily by the lowest mode, which has a global shape, whereas the application of dampers predominantly affects higher mode shapes that are more localized.

Fig. 25 offers an initial assessment of how the base angle influences displacement in gridshells equipped with VE dampers. The trendlines suggest a general shift toward more ellipsoidal shapes (i.e., positive base angle deviation) as optimal under seismic loading. To better distinguish the effect of damper quantity, Fig. 26 plots maximum displacement against base angle deviation, using a colormap to indicate the number of applied VE dampers. This visualization reveals that the relationship between base angle and displacement is not fixed but evolves with increasing damper quantity.

Fig. 27, which extracts trendlines from the data in Fig. 26, further clarifies this behavior: in uncontrolled models or those with a low

Table 9
Optimization information of opt. 3a, locally symmetric topologies.

Variable input parameters	Range of variation	Optimization objective
Height (Control points' elevation)	9.75–20.25 m (13–27 m)	
Base tangent inclination (Control points' distance)	35–70° (11.5–21.5 m)	Minimize peak resultant displacement
Dampers' Configuration (locally symmetric topologies)	0–31	

Table 10
Optimal locally symmetric topologies, '0': normal member, '1': VE damper member.

Topology ID	Diagonal member as noted in Fig. 5										Total applied dampers	Scheme
	1	2	3	4	5	6	7	8	9	10		
7	0	0	1	1	1	1	1	1	0	0	48	
11	0	1	0	1	1	1	1	0	1	0	48	
15	0	1	1	1	1	1	1	1	1	0	64	
23	1	0	1	1	1	1	1	1	0	1	64	

Table 11
Effect of damper application on the dominant period and maximum displacement of dome structures in four representative topologies. Heights and angle deviations from arc are included for reference.

Topology ID	Height (m)	Angle Dev. (°)	Dominant Period (Unctrl.) (s)	Dominant Period (Ctrl.) (s)	Max Disp. (Unctrl.) (mm)	Max Disp. (Ctrl.) (mm)
7	14	0	0.11	1.23	73.2	43.2
11	14	1.5	0.11	0.89	73.3	42.7
15	15.5	2	0.4	1.68	63.2	42.8
23	14	1.5	0.11	1.34	73.3	39.1

number of dampers, the optimal base angle tends to lie near or below the arc reference (0°), aligning with more funicular geometries. In contrast, as the number of dampers exceeds 32, the optimal base angle shifts progressively toward higher values, favoring ellipsoidal forms. This indicates that the introduction of dampers not only reduces displacement but also alters the structural preference for dome geometry.

The use of VE dampers in the first ring of Kiewitt-8 gridshell domes significantly reduces the maximum deformations, which are strongly influenced by the higher-period modes in the uncontrolled structure. The VE dampers effectively shift the dominant mode (namely the 1st mode) to longer periods, placing it outside the earthquake predominant period. While increasing the structural period lowers the acceleration according to the acceleration response spectrum, it also results in increased deformations as indicated by the displacement response spectrum. However, the inherent damping properties of the VE dampers successfully control and mitigate these additional displacements.

Conversely, VE dampers tend to have minimal impact on the dominant period of shallow domes (those with a low height-to-span ratio), as the lower-period mode remains the dominant mode, and this mode shape is not substantially affected by the dampers implementation. Additionally, due to the higher geometrical stiffness of shallow domes, replacing diagonal elements with dampers significantly reduces their overall stiffness. In some cases, this reduction can lead to increased deformations, as predicted by the displacement response spectrum, ultimately outweighing the damping benefits of the VE dampers.

In optimizing the maximum displacement of the Kiewitt-8 gridshell dome, which is influenced by both global and local structural responses, no singular combination of height, base tangent inclination, or damper topology consistently emerges as optimal. Rather, a spectrum of viable solutions emerges, underscoring the need for a comprehensive evaluation. Notably, Fig. 28 synthesizes the results across all considered earthquake records, where each bar represents the range of maximum displacements observed for each of the 32 locally symmetric topologies (indicated on the abscissa). Among all locally symmetric topologies of Fig. 6 evaluated across the seven earthquake accelerograms listed in Fig. 9, configurations 7, 11, 15, and 23 stand out for their combination of low maximum displacements and reduced response variability across seismic events, indicating consistent performance across different seismic events. Table 10 presents the detailed genome configuration patterns and schematic representations of these high-performing topologies.

Given the large solution space for damper topology, additional factors could also be considered, such as the disparity of maximum displacement, and the maximum horizontal support reaction force associated with each damper configuration. Notably, Figs. 29 and 30 serve as illustrative examples from a series of time history analyses conducted subjected to seven earthquake records, specifically detailing the outcomes for the Northridge and Landers records. For instance, Figs. 29a and 30a are detailed scatter plots from which, together with the other five records results, produced Fig. 28. These figures indicate configurations 7, 11, 15, and 23 (shown in Table 10) as particularly effective, characterized by consistent low displacements, and are highlighted in the plot with different colors.

Furthermore, as illustrated in Figs. 29c and 30c, these configurations are also advantageous in generating the lowest maximum horizontal support reaction forces, adding another layer of benefit to their selection. Figs. 29b and 30b show how the base tangent inclination tends to have an angle over the corresponding arc which is also shown in Fig. 25 for all the records. Similarly, the selection of appropriate damper topologies and an increase in base tangent inclination contribute to a reduction in the maximum horizontal support reaction force, as evidenced by Figs. 29d and 30d.

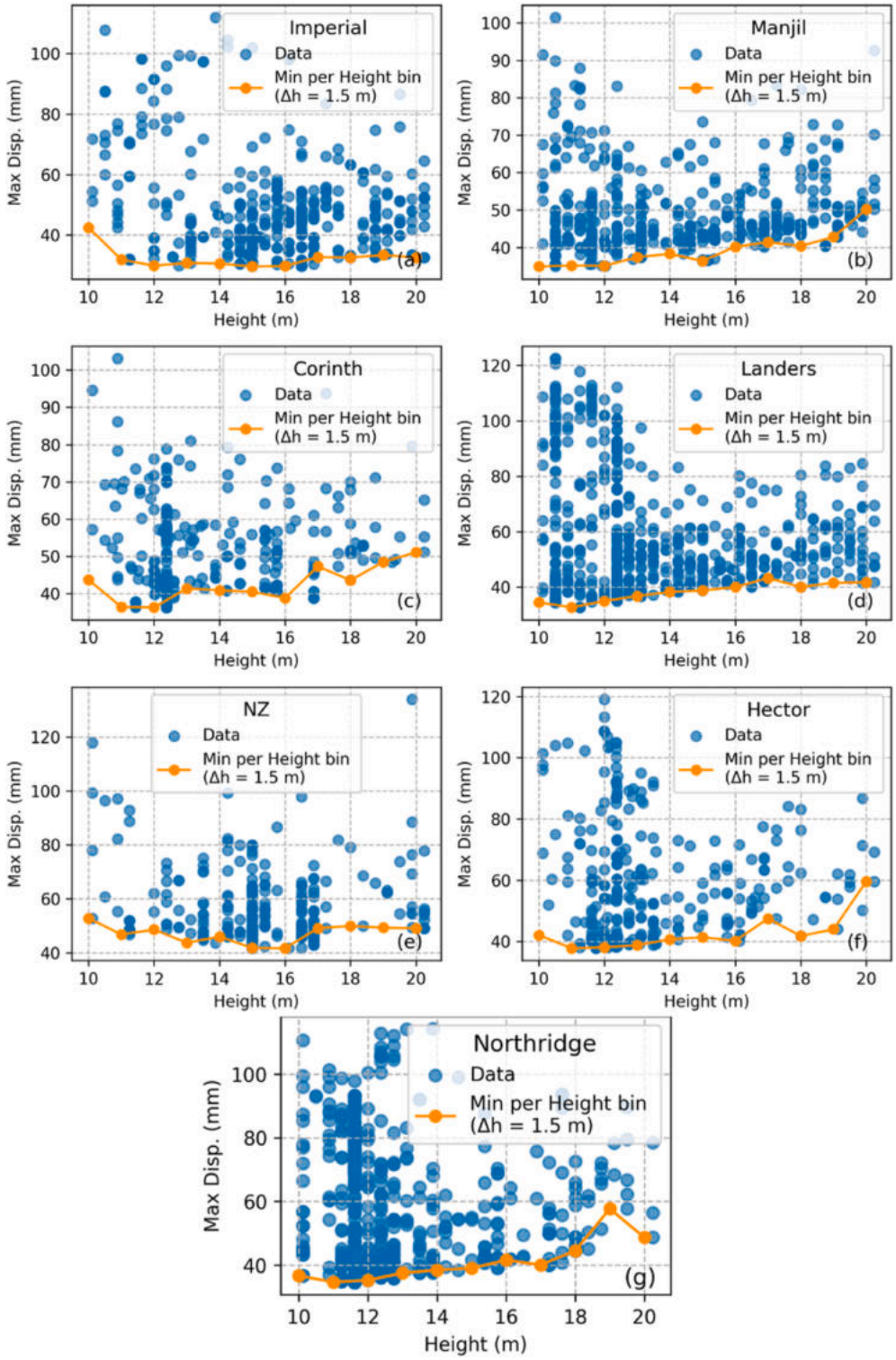

Fig. 23. Maximum displacement of the controlled model as a function of dome height. Trendlines represent the minimum observed displacement within each 1.5 m height bin, illustrating general performance trends across varying structural heights.

The design algorithm for the gridshell dome can be summarized based on the observed mode shapes and their influence under different geometric configurations. As shown in Fig. 18, the studied uncontrolled gridshell dome exhibits two primary mode shapes: a lower period ranging between 0.10 and 0.14 s and a higher period between 0.40 and 0.50 s. For very shallow domes, with an R/S ratio

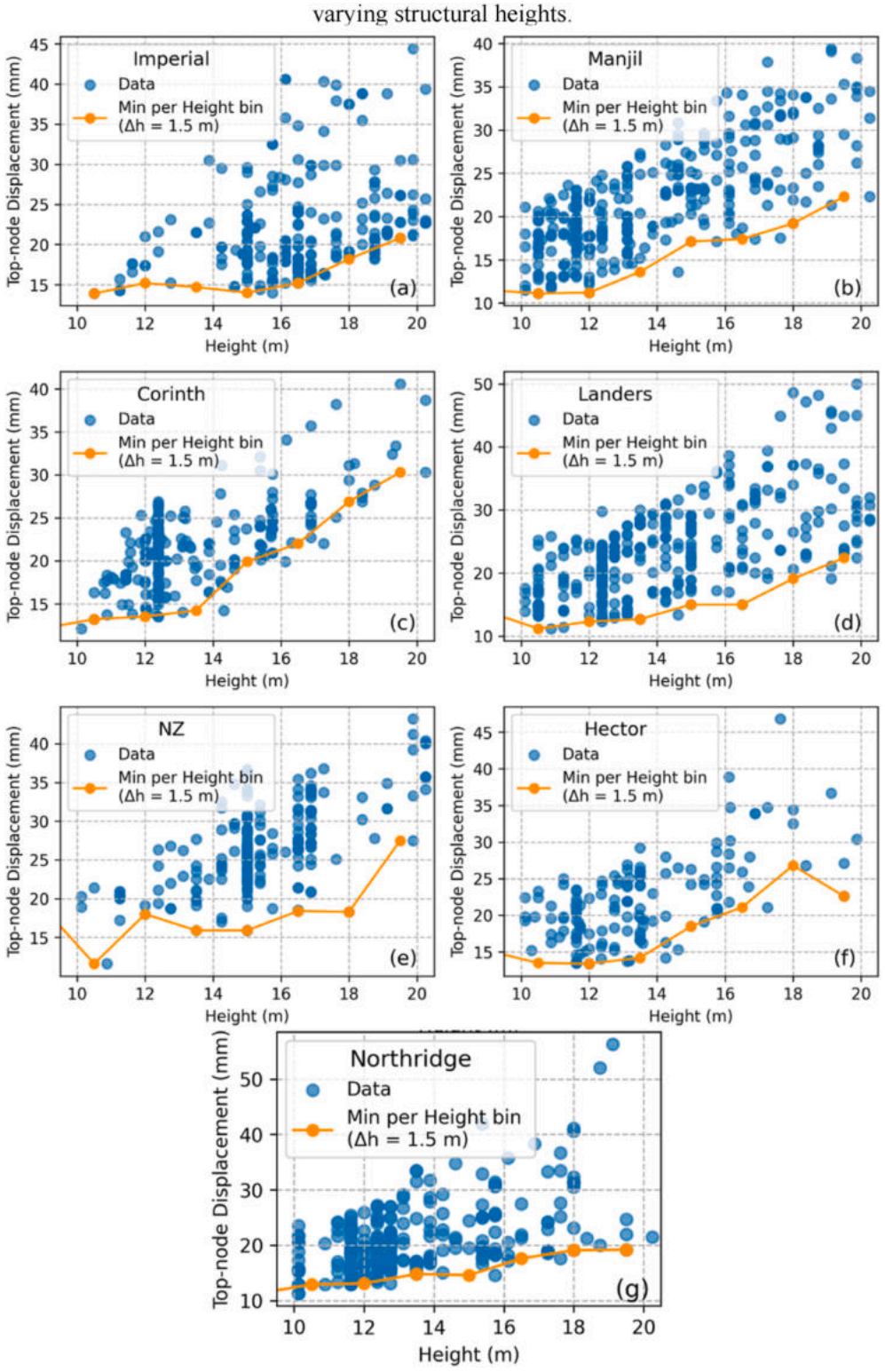

Fig. 24. Maximum top-node displacement of the controlled model as a function of dome height. Trendlines represent the minimum observed displacement within each 1.5 m height bin, illustrating general performance trends across varying structural heights.

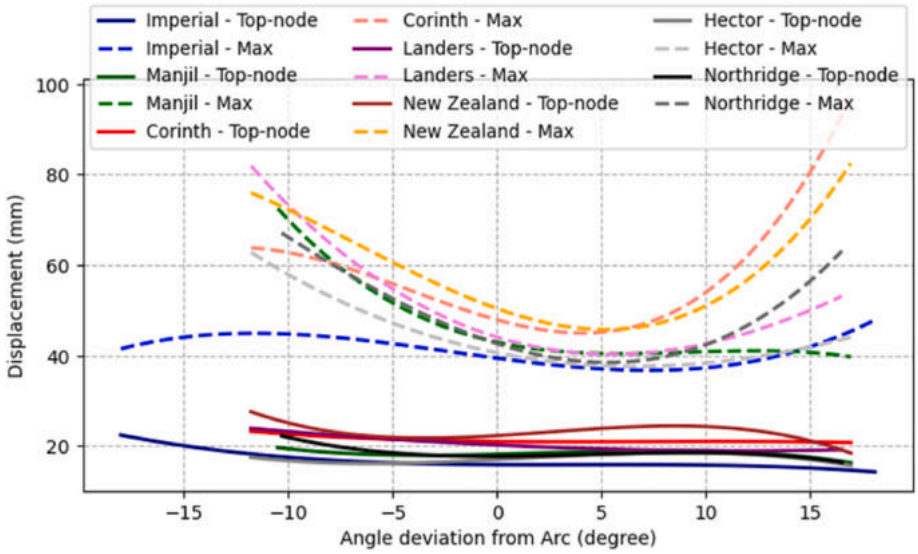

Fig. 25. Maximum and top-node displacement vs. base angle deviation for controlled models under different earthquake records.

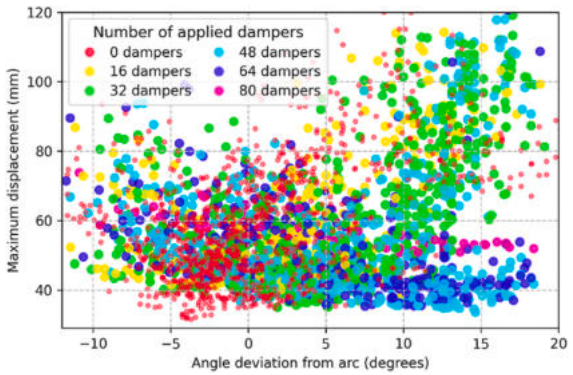

Fig. 26. Maximum displacement vs. base angle deviation for all controlled models. Color indicates the number of applied VE dampers.

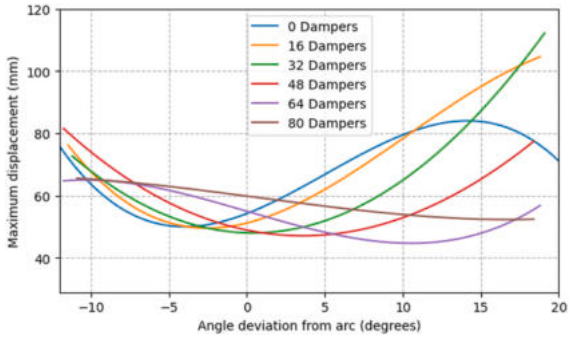

Fig. 27. Trendlines of maximum displacement vs. base angle deviation, grouped by damper quantity.

of less than 1/5, the dominant period is within the lower period range. In these cases, the base tangent inclination has minimal influence on maximum displacement. Since the lower period is so dominant, removing diagonal members does not significantly alter the dominant period. Consequently, the addition of VE dampers is mostly ineffective, as the dome's deformation is already low, leaving little opportunity for the dampers to dissipate seismic energy. Replacing diagonal members with VE dampers is therefore not a suitable strategy for shallow domes.

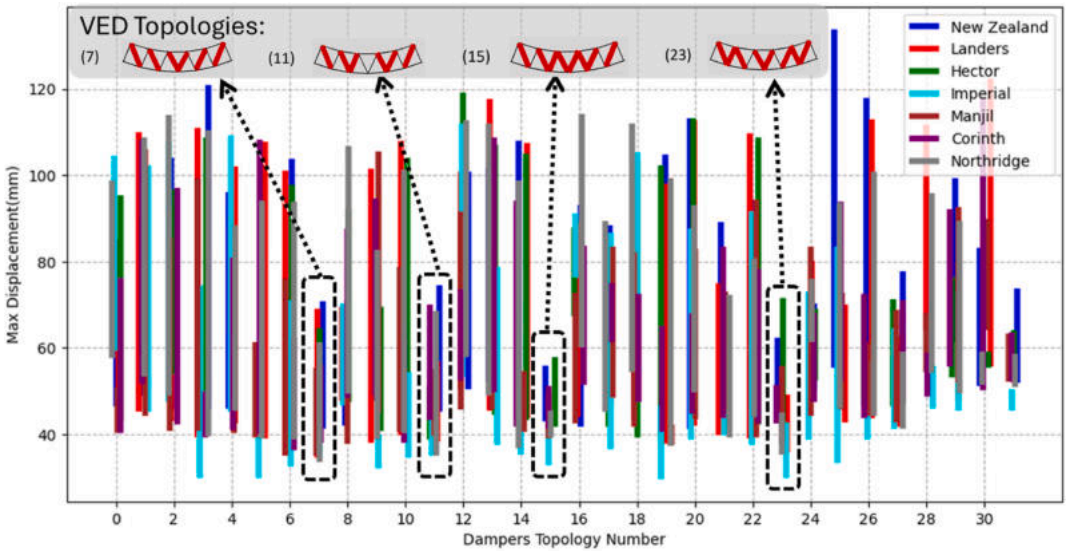

Fig. 28. Range of variation of Maximum displacement per dampers' topology.

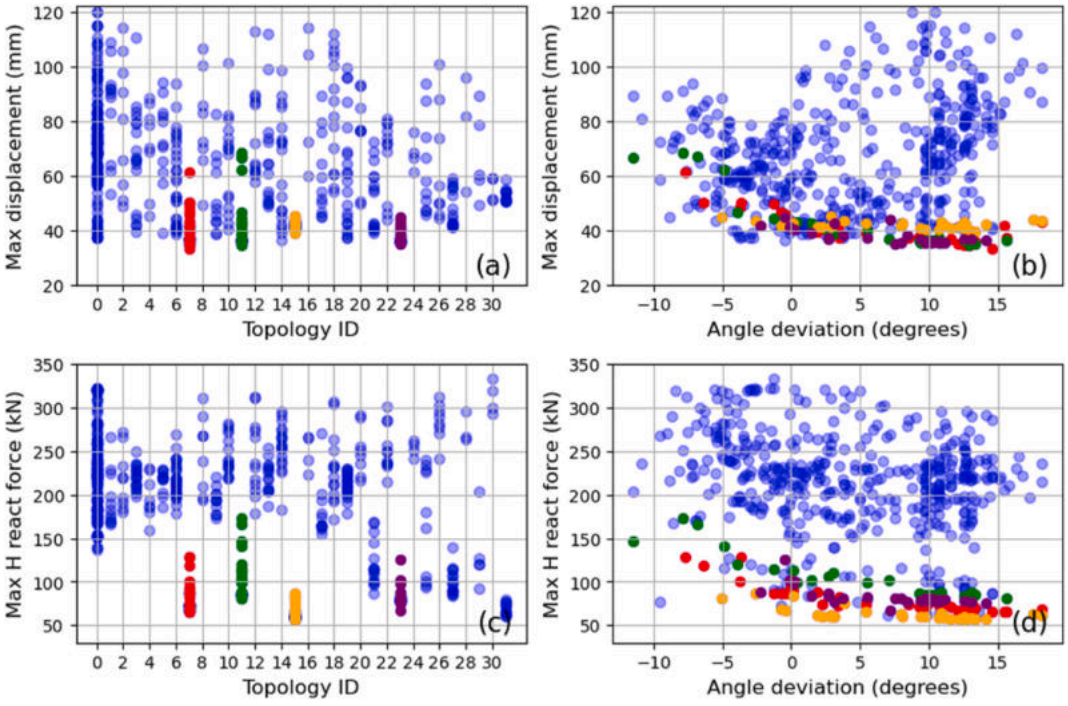

Fig. 29. Analysis results for the Northridge record using locally symmetric VE dampers, with indicated damper topologies (7: red, 11: green, 15: yellow, 23: purple); (a) Maximum displacement vs. topology ID; (b) Maximum displacement vs. base angle deviation from the corresponding arc; (c) Maximum horizontal reaction force vs. topology ID; (d) Maximum horizontal reaction force vs. base angle deviation from the corresponding arc.

For mid-height domes, with an R/S ratio between 1/5 and 1/4, the base tangent inclination becomes more significant, and either the lower or higher period can dominate, depending on the dome's specific geometry. If the higher period is dominant, the maximum displacement in the uncontrolled model may be substantial. In this case, replacing diagonal members with VE dampers effectively shifts the dominant period to higher values, reducing its sensitivity to seismic events and allowing the dampers to dissipate energy more effectively. If the lower period is dominant, the dome's behavior depends on the number of dampers applied. With fewer dampers (e.g., 8 or 16), the gridshell behaves similarly to the uncontrolled model, maintaining a dominant period between 0.11 and 0.15 s. However, applying a larger number of dampers (above 24) may shift the dominant period to the higher one (Fig. 31). This dominant

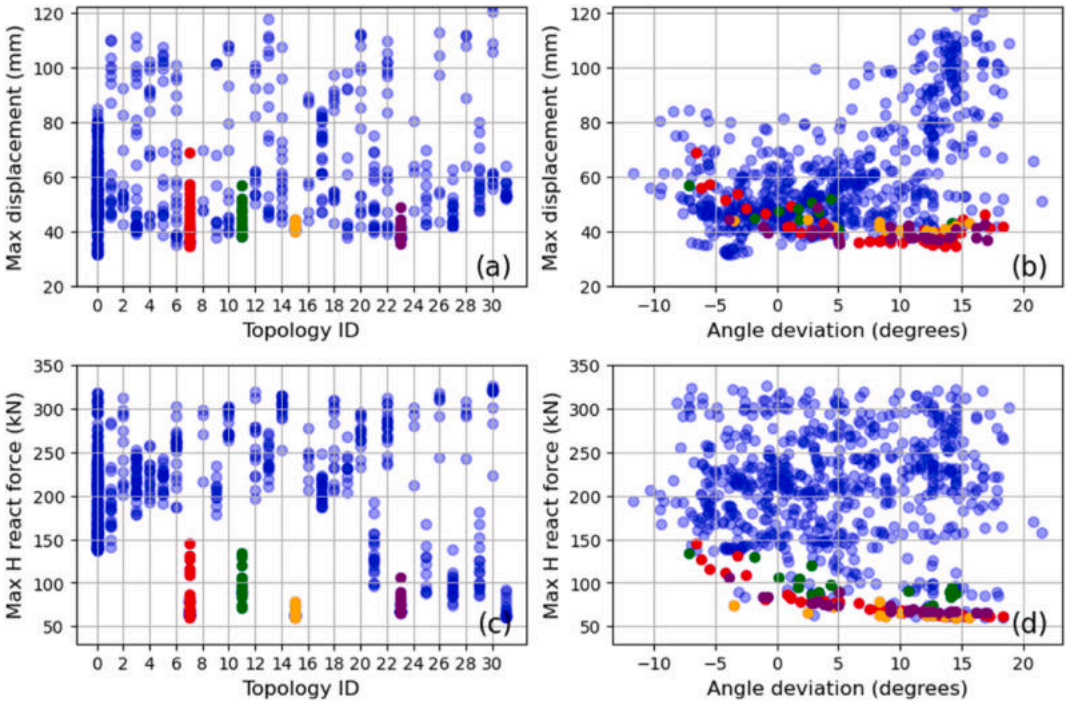

Fig. 30. Analysis results for the Landers record using locally symmetric VE dampers, with highlighted damper topologies (7: red, 11: green, 15: yellow, 23: purple); (a) Maximum displacement vs topology ID; (b) Maximum displacement vs base angle deviation from the corresponding arc; (c) Maximum horizontal reaction force vs topology ID; (d) Maximum horizontal reaction force vs base angle deviation from the corresponding arc.

mode transition from a global shape mode to a local shape mode may help in reducing the maximum displacement of the dome as well. Table 11 presents the change in dominant period and maximum displacement for the four most optimal topologies of specific dome shapes, where a noticeable increase in period and a reduction in displacement are observed due to damper application.

For taller gridshell domes, with an R/S ratio between 1/4 and 1/3, the higher period is more likely to dominate. This results in greater structural deformation. Similar to mid-height domes where the higher period dominates, the application of VE dampers is effective in reducing maximum displacement by shifting the dominant period to less seismic-sensitive ranges. However, it is important to note that the overall trend indicates that maximum displacement increases with dome height and fundamental period. As a result, applying dampers to domes that already exhibit high dominant periods may lead to amplified deformations, while the additional damping effect remains limited.

As a sample case, the 12 m height gridshell dome illustrates the effect of VE dampers. In the uncontrolled model (see Fig. 18), the lower and higher mode shape periods are 0.12 s (dominant mode) and 0.41 s, respectively. In the controlled model with the same height and span (see Fig. 32), but equipped with VE dampers in topology ID 7, the higher mode shape period shifts to 1.25 s (dominant mode), well beyond the predominant excitation period of all seismic records, while the lower mode shape period remains relatively

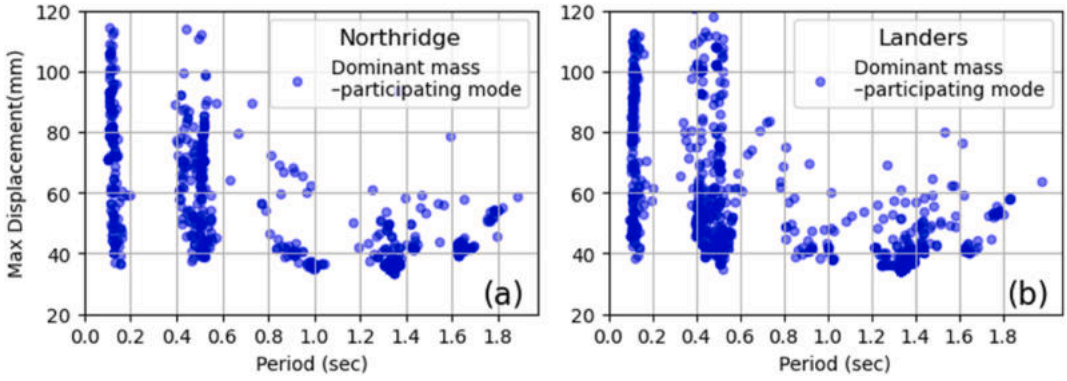

Fig. 31. Comparison of maximum displacement vs. the dominant mass-participation mode's period of controlled models with locally symmetric damper topologies under Northridge and Landers earthquake records.

low at 0.14 s.

In summary, replacing structural members in the first ring of the Kiewitt-8 gridshell with VE dampers produces two main effects: First, the overall period of the structure is modified due to a reduction in global stiffness. Second, while allowing for greater structural movements, the dampers absorb energy through their inherent damping properties, leading to a further reduction in displacement.

By finally considering all possibilities of damper topologies (locally both symmetric and asymmetric), in optimization scenario 3b (opt. 3b), optimization of damper configuration in the first ring, alongside adjustments to height and base tangent inclination, can result in a vast number of iterations to achieve the best outcome, owing to the huge number of possible layouts (Table 12). To minimize the computation time, the variation intervals for height and base tangent inclination are broadened. Table 12 shows the variables and their range of variations. The full optimization process, including locally asymmetric damper topologies, required approximately 7635 min to complete. Under the Hector seismic records, this optimization strategy results in a reduced optimal maximum resultant displacement of 32 mm, an improvement over the 37 mm displacement observed with locally symmetric VE damper allocations—both outcomes being within acceptable limits. However, while locally asymmetric damper configurations demonstrate enhanced performance, two critical issues emerge: the time required for analyzing locally asymmetric topologies markedly increases compared to symmetric ones, and the maximum horizontal support reaction forces are generally higher in optimal locally asymmetric configurations than in their symmetric counterparts.

The optimization analysis (Fig. 33) of this section verifies findings from earlier analyses regarding displacement variations when adjusting the height and base tangent inclination. This is further illustrated in Fig. 34 for the Hector earthquake record, with similar trends are observed across all earthquake scenarios analyzed. Fig. 35 illustrates the optimal height and base tangent inclination range for models on which the VE dampers are applied.

Table 13 presents the nine most effective damper configurations identified across the seven earthquake records analyzed. These top-performing solutions feature between 32 and 48 VE dampers. While configurations with 32 dampers offer a more cost-effective option, those employing 40 or 48 dampers tend to deliver more consistent and reliable performance across different dome geometries. Fig. 36 plots the maximum displacement values for all tested topologies across all records under optimization scenario 3b. The highlighted points correspond to the nine configurations listed in Table 13, which consistently achieve among the lowest displacement values within the explored design space. This confirms their superior performance relative to the broader set of configurations examined in this scenario.

6. Conclusions

Providing further insights for design decision-making, this study introduces a design methodology that integrates structural analysis into the early design stage, optimizing both the shape of the gridshell structure and the configuration of viscoelastic (VE) dampers. While studies have shown that VE dampers are effective in reducing seismic responses, their influence on optimal gridshell geometry remains insufficiently explored. This work addresses that gap by demonstrating how the inclusion of dampers affects both seismic performance and the gridshell's structural form. By employing parametric design and genetic algorithm optimization, the proposed approach addresses the nonlinear problem of simultaneous shape and damper placement optimization. Utilizing multi-phase optimization, the nonlinear time-history analysis plays a central role in the fitness function, capturing dynamic responses, damping effects, and material and geometric nonlinearities.

Applying this methodology to Kiewitt-8 gridshell domes demonstrates that the optimal shape of uncontrolled and controlled gridshell domes differs and depends on the number of applied dampers. Thus, the optimal shape becomes increasingly elliptical as more dampers are implemented. VE dampers improve structural performance by reducing maximum displacement and thrust forces at the dome's base. Maximum displacement is reduced by over 50 %, with optimized configurations achieving values of 30–40 mm compared to 60–80 mm in the uncontrolled model. Similarly, the thrust forces decrease by up to 40 %.

Replacing diagonal elements with VE dampers shifts the dominant mode period, moving it outside the predominant period range of earthquake ground motions, and reducing the seismic response. Gridshell domes with a mid rise-to-span ratio benefit the most from this method, while shallow domes show limited improvement due to the dominance of the lower-period mode. The inherent damping of the VE dampers effectively mitigates additional displacements caused by period elongation, particularly in mid-to high-rise gridshells. However, the influence of an excessively long dominant period should be carefully considered, as it may lead to undesirable

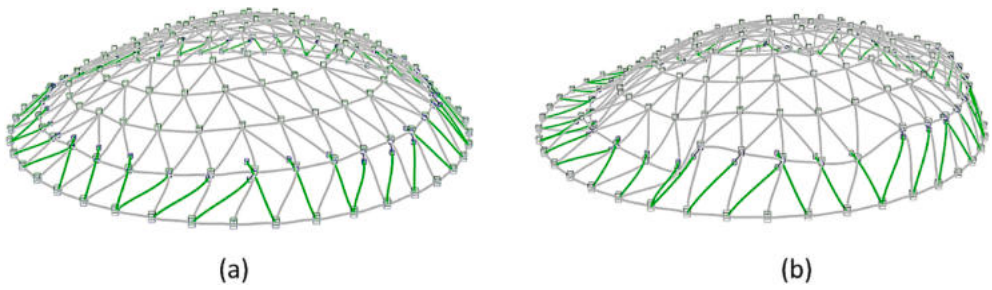

Fig. 32. Mode shapes of the controlled model (Topology ID 7 with 48 VE dampers) (members in green have dampers) (a) Shape mode with lower period (T = 0.14 s) (b) Shape mode with higher period (T = 1.23 s).

Table 12
Optimization information of opt. 3b, all possible topologies.

Variable input parameters	Range of variation	Optimization objective
Height (Control points' elevation)	9.75–20.25 m (13–27)	
Base tangent inclination (Control points' distance)	35–70° (11.5–21.5)	Minimize peak resultant displacement
Dampers' Configuration (all topologies)	0–1023	

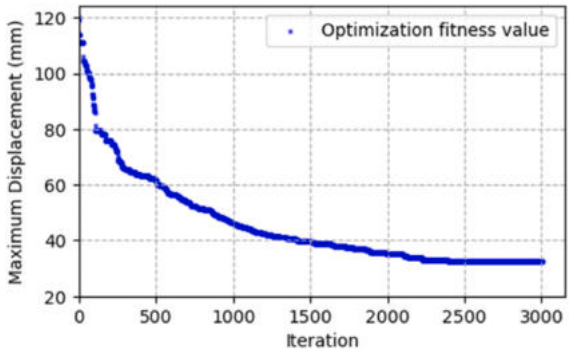

Fig. 33. Optimization process outcome under Hector record.

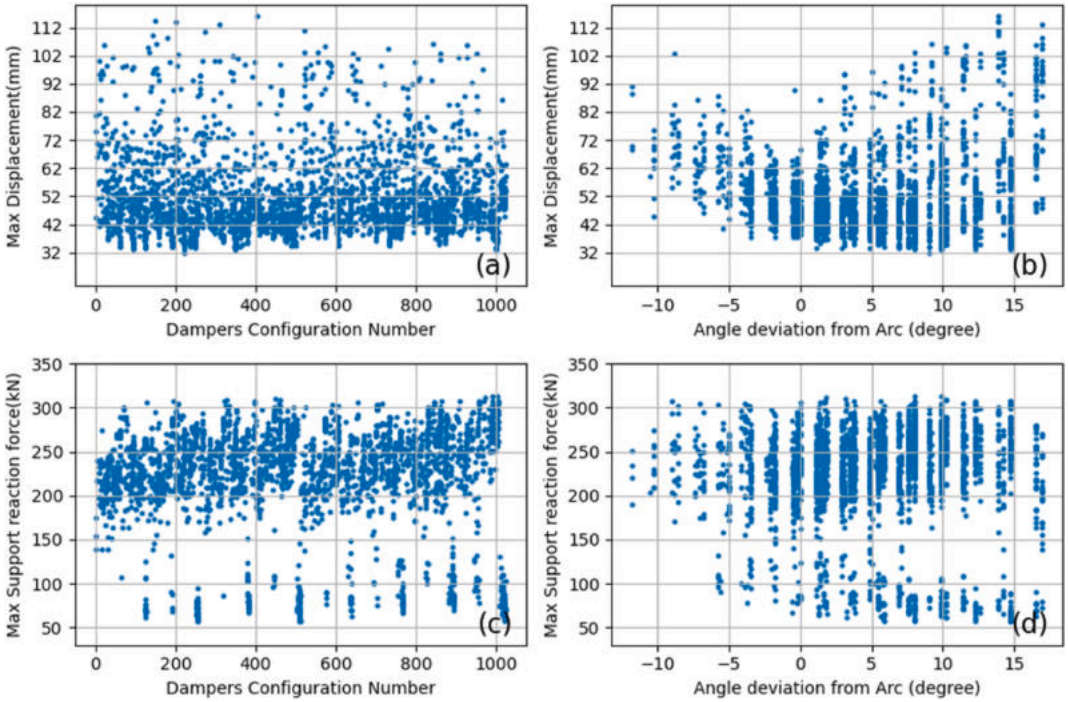

Fig. 34. Hector record analysis results utilizing VE dampers (all topologies); (a) Maximum displacement vs topology ID; (b) Maximum displacement vs base angle deviation from the corresponding arc; (c) Maximum horizontal reaction force vs topology ID; (d) Maximum horizontal reaction force vs base angle deviation from the corresponding arc.

deformations. Therefore, the application of VE dampers through this methodology is not advised for domes exceeding 18 m in height.

The optimal number of dampers ranges between 32 and 64, with symmetric configurations achieving consistent reductions in both maximum displacement and base reaction forces across various seismic records. Locally asymmetric layouts may yield slightly better displacement reductions in specific scenarios, but often increase horizontal support reactions due to uneven force distribution. Additionally, incorporating all possible topologies in the optimization process significantly increases computational time.

VE dampers also reduce member stresses and deformations, potentially allowing for smaller section sizes and lighter structures,

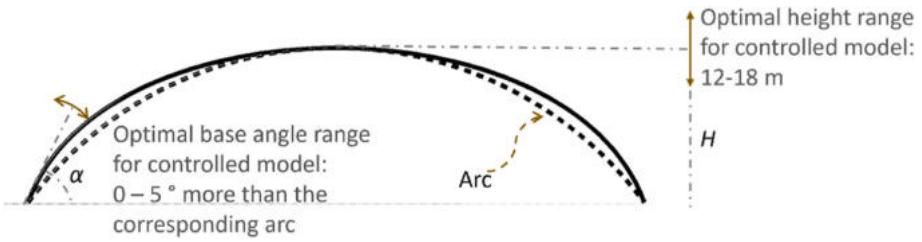

Fig. 35. Optimal height and base angle range for controlled model.

Table 13
Optimal topologies, '0': normal member, '1': VE damper member.

Topology ID	Diagonal member as noted in Fig. 17										Total applied dampers	Scheme
	1	2	3	4	5	6	7	8	9	10		
190	0	0	1	0	1	1	1	1	1	0	48	
222	0	0	1	1	0	1	1	1	1	0	48	
94	0	0	0	1	0	1	1	1	1	0	40	
606	1	0	0	1	0	1	1	1	1	0	48	
30	0	0	0	0	0	1	1	1	1	0	32	
236	0	0	1	1	1	0	1	1	0	0	40	
62	0	0	0	0	1	1	1	1	1	0	40	
350	0	1	0	1	0	1	1	1	1	0	48	

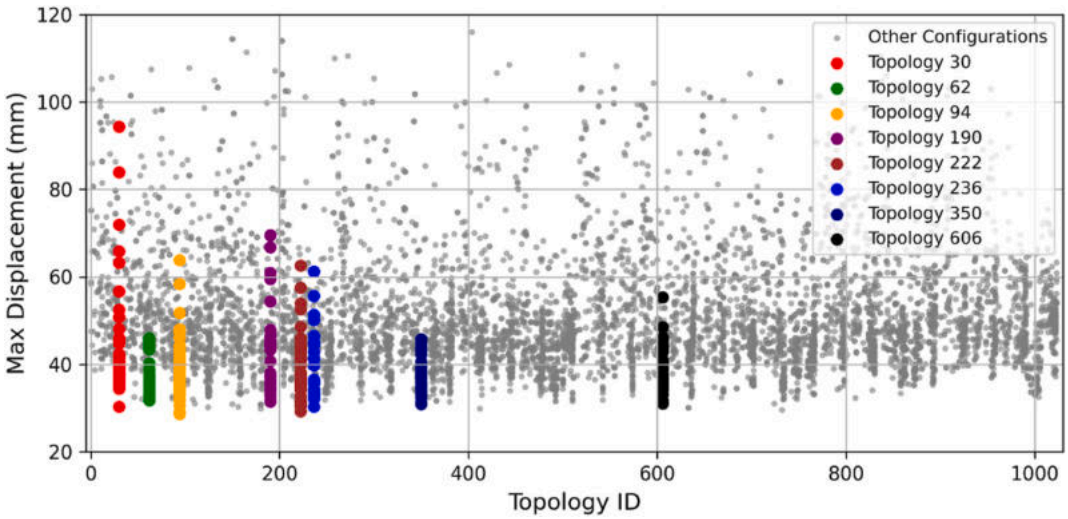

Fig. 36. Maximum displacement versus damper topology IDs for all analyzed records. Highlighted points represent selected damper topologies of interest.

though further investigation is required to quantify material savings. This reduction in material usage could help offset the cost of the VE dampers. However, since satisfactory structural performance is achieved with fewer dampers (e.g., 32), it is recommended to use the minimum number necessary to avoid unnecessary expenses.

In conclusion, this framework not only improves the seismic performance of gridshell domes but also demonstrates the importance of considering both geometry and damping systems in the early design stage. It offers a robust and adaptable tool for the design of gridshell domes and other structures, contributing to safer and more efficient building practices.

The results suggest the following design considerations.

- Optimal Shape: When VE dampers replace diagonal elements, the optimal shape of a gridshell dome often shifts from a parabola-like form to a more ellipsoidal form, which helps minimize both displacements and thrust forces.
- Number of Dampers: The optimal number of dampers typically ranges between 32 and 64, though considering cost effects, fewer dampers are preferred.
- Period Change: Replacing structural elements with VE dampers increases the dominant mode period, reducing seismic response, particularly in domes with higher rise-to-span ratios.
- Dome Height: VE damper performance is most effective in domes with rise-to-span ratios between approximately 1/5 and just above 1/4. Displacement reduction is less effective in shallow domes (R/S close to 1/6) due to lower mode dominance. For domes with R/S ratios close to 1/3 (e.g., over 18 m), period elongation may lead to excessive deformations, making this approach less suitable.
- Symmetry vs. Asymmetry: While locally asymmetric damper layouts can achieve slightly better displacement reductions, optimal symmetric layouts provide better control over thrust forces, which may be crucial depending on the design objectives.

Future research could expand the application of this design methodology to a wider range of structures that allow shape optimization while adding a vibration control device. Additionally, the minimization of different objectives, such as cost, could be another approach to developing the study. Moreover, while in this study, a two-phase optimization was used considering static and dynamic analysis, a further dedicated multiphase approach could help remove the poor individuals before the time-history analysis which is time-consuming.

CRediT authorship contribution statement

Alireza Hosseini: Writing – original draft, Validation, Software, Methodology, Formal analysis, Data curation, Conceptualization. **Bruno Briseghella:** Writing – review & editing, Validation, Supervision, Methodology, Conceptualization. **Gian Felice Giaccu:** Writing – review & editing, Validation, Methodology, Conceptualization. **Luigi Fenu:** Writing – review & editing, Writing – original draft, Validation, Supervision, Project administration, Methodology, Funding acquisition, Conceptualization.

Declaration of competing interest

The authors declare that they have no known competing financial interests or personal relationships that could have appeared to influence the work reported in this paper.

Acknowledgments

This work was supported by the Italian Ministry of University and Research (MIUR), PhD Operational National Program in Research and Innovation (PON RI) XXXV Cycle, CUP: F25J19000600007.

Data availability

No data was used for the research described in the article.

References

[1] H. Pottmann, A. Asperl, A. Kililan, Architectural Geometry, Bentley Institute Press, Philadelphia, PA, 2007, https://doi.org/10.1137/1.9781934493045.
[2] S. Adriaenssens, P. Block, D. Veenendaal, C. Williams, Shell Structures for Architecture; Form Finding and Optimization, Routledge, 2014, https://doi.org/10.4324/9781315849270.
[3] T. Saka, Y. Taniguchi, Damage to spatial structures by the 1995 hyogoken-nanbu earthquake in Japan, Int. J. Space Struct. 12 (1997) 125–133.
[4] X. Zhi, F. Fan, S. Shen, Elasto-plastic instability of single-layer reticulated shells under dynamic actions, Thin-Walled Struct. 48 (2010) 837–845, https://doi.org/10.1016/j.tws.2010.04.005.
[5] R.V. Vazna, M. Zarrin, Sensitivity analysis of double layer diamatic dome space structure collapse behavior, Eng. Struct. 212 (2020) 110511, https://doi.org/10.1016/j.engstruct.2020.110511.
[6] L.J. Li, Z.H. Xie, Y.C. Guo, F. Liu, Structural optimization and dynamic analysis for double-layer spherical reticulated shell structures, J. Constr. Steel Res. 62 (2006) 943–949, https://doi.org/10.1016/j.jcsr.2006.01.010.
[7] L min Tian, C. Bai, W hui Zhong, Experimental study and numerical simulation of partial double-layer latticed domes against progressive collapse in member-removal scenarios, Structures 29 (2021) 79–91, https://doi.org/10.1016/j.istruc.2020.10.082.
[8] Wei J. peng, Tian L. min, J ping Hao, Improving the progressive collapse resistance of long-span single-layer spatial grid structures, Constr. Build. Mater. 171 (2018) 96–108, https://doi.org/10.1016/j.conbuildmat.2018.03.126.

[9] T.T. Soong, M.C. Costantinou, Passive and Active Structural Vibration Control in Civil Engineering, Springer-Verlag Wien GmbH, 1994, https://doi.org/10.1007/978-3-7091-3012.
[10] I.D. Aiken, J.M. Kelly, Experimental and Analytical Studies of Two energy-absorbing Systems for Multistory Structures, 1991.
[11] Z.D. Xu, Y.F. Guo, S.A. Wang, X.H. Huang, Optimization analysis on parameters of multi-dimensional earthquake isolation and mitigation device based on genetic algorithm, Nonlinear Dyn. 72 (2013) 757–765, https://doi.org/10.1007/s11071-013-0751-9.
[12] A.K. Shukla, T.K. Datta, Optimal use of viscoelastic dampers in building frames for seismic force, J. Struct. Eng. 125 (1999) 401–409.
[13] Y. Yang, B. Spencer, Y. Li, S. Shen, Seismic performance of double-layer spherical reticulated shell with replaceable bar-type dampers, Int. J. Space Struct. 26 (2011) 31–44, https://doi.org/10.1260/0266-3511.26.1.31.
[14] W. Liu, J. Ye, Collapse optimization for domes under earthquake using a genetic simulated annealing algorithm, JCSR 97 (2014) 59–68, https://doi.org/10.1016/j.jcsr.2014.01.015.
[15] S. Yan, X. Zhao, K.J.R. Rasmussen, H. Zhang, Identification of critical members for progressive collapse analysis of single-layer latticed domes, Eng. Struct. 188 (2019) 111–120, https://doi.org/10.1016/j.engstruct.2019.03.027.
[16] F. Fan, Z. Cao, S. Shen, Elasto-plastic stability of single-layer reticulated shells, Thin-Walled Struct. 48 (2010) 827–836, https://doi.org/10.1016/j.tws.2010.04.004.
[17] V.B. Patil, R.S. Jangid, Response of wind-excited benchmark building installed with dampers, Struct. Des. Tall Special Build. 20 (2011) 497–514, https://doi.org/10.1002/tal.523.
[18] E. Aydin, Optimal damper placement based on base moment in steel building frames, J. Constr. Steel Res. 79 (2012) 216–225, https://doi.org/10.1016/j.jcsr.2012.07.011.
[19] F. Amini, P. Ghaderi, Hybridization of harmony search and ant colony optimization for optimal locating of structural dampers, Appl. Soft Comput. J. 13 (2013) 2272–2280, https://doi.org/10.1016/j.asoc.2013.02.001.
[20] A.K. Agrawal, J.N. Yang, Optimal placement of passive dampers on seismic and wind excited buildings using combinatorial, Intell. Mater. Sys. Struct. 10 (1999).
[21] M.P. Singh, L.M. Moreschi, Optimal placement of dampers for passive response control, Earthq. Eng. Struct. Dynam. 31 (2002) 955–976, https://doi.org/10.1002/eqe.132.
[22] G. Angelucci, F. Mollaioli, R. Tardocchi, A new modular structural system for tall buildings based on tetrahedral configuration, Buildings 10 (2020) 1–22, https://doi.org/10.3390/buildings10120240.
[23] G. Angelucci, G. Quaranta, F. Mollaioli, Topology optimization of multi-story buildings under fully non-stationary stochastic seismic ground motion, Struct. Multidiscip. Optim. 65 (2022), https://doi.org/10.1007/s00158-022-03319-5.
[24] Z.D. Xu, H.T. Zhao, A.Q. Li, Optimal analysis and experimental study on structures with viscoelastic dampers, J. Sound Vib. 273 (2004) 607–618, https://doi.org/10.1016/S0022-460X(03)00522-4.
[25] E. Tubaldi, M. Barbato, A. Dall'Asta, Performance-based seismic risk assessment for buildings equipped with linear and nonlinear viscous dampers, Eng. Struct. 78 (2014) 90–99, https://doi.org/10.1016/j.engstruct.2014.04.052.
[26] D. Zhou, Y. Bao, C. Huang, Y.J. Zhao, Semi-active direct velocity control method for dynamic response of spatial reticulated structures, Adv. Struct. Eng. 12 (2009) 547–558.
[27] Y. Yang, H. Ma, Optimal topology design of replaceable bar dampers of a reticulated shell based on sensitivity analysis, Earthq. Eng. Eng. Vib. 13 (2014) 113–124, https://doi.org/10.1007/s11803-014-0216-2.
[28] J. Xu, S. Xu, Z. Yuan, Probabilistic seismic analysis of single-layer reticulated shell structures controlled by viscoelastic dampers with an effective placement, Eng. Struct. 222 (2020), https://doi.org/10.1016/j.engstruct.2020.111052.
[29] A. Manguri, N. Saeed, F. Kazemi, M. Szczepanski, R. Jankowski, Optimum number of actuators to minimize the cross-sectional area of prestressable cable and truss structures, Structures 47 (2023) 2501–2514, https://doi.org/10.1016/j.istruc.2022.12.031.
[30] F. McKenna, M.H. Scott, G.L. Fenves, Nonlinear finite-element analysis software architecture using object composition, J. Comput. Civ. Eng. 24 (2010) 95–107.
[31] M.E. Mortenson, Mathematics for Computer Graphics Applications, Industrial Press Inc, 1999.
[32] M. Zhu, F. McKenna, M.H. Scott, OpenSeesPy: python library for the OpenSees finite element framework, SoftwareX 7 (2018) 6–11, https://doi.org/10.1016/j.softx.2017.10.009.
[33] M.F. Ferrotto, L. Fenu, J.Q. Xue, B. Briseghella, B.C. Chen, L. Cavaleri, Simplified equivalent finite element modelling of concrete-filled steel tubular K-joints with and without studs, Eng. Struct. 266 (2022), https://doi.org/10.1016/j.engstruct.2022.114634.
[34] J. Wardenier, Hollow Sections in Structural Applications. CIDECT, Bouwen met Staal, 2010.
[35] W. Huang, L. Fenu, B. Chen, B. Briseghella, Experimental study on K-joints of concrete-filled steel tubular truss structures, J. Constr. Steel Res. 107 (2015) 182–193, https://doi.org/10.1016/j.jcsr.2015.01.023.
[36] Eurocode 3, Design of Steel Structures. EN 1993, 2005. Brussels.
[37] A.K. Chopra, Dynamic of Structures, Theory and Applications to Earthquake Engineering, 2012.
[38] G. Pekcan, J.B. Mander, S.S. Chen, Fundamental considerations for the design of non-linear viscous dampers, Earthq. Eng. Struct. Dynam. 28 (1999) 1405–1425, https://doi.org/10.1002/(SICI)1096-9845(199911)28:11<1405::AID-EQE875>3.0.CO;2-A.
[39] F. Kazemi, B. Mohebi, R. Jankowski, Predicting the seismic collapse capacity of adjacent SMRFs retrofitted with fluid viscous dampers in pounding condition, Mech. Syst. Signal Process. 161 (2021), https://doi.org/10.1016/j.ymssp.2021.107939.
[40] A. Dall'asta, E. Tubaldi, L. Ragni, Influence of the nonlinear behavior of viscous dampers on the seismic demand hazard of building frames, Earthq. Eng. Struct. Dynam. 45 (2016) 149–169, https://doi.org/10.1002/eqe.2623.
[41] A. Yahyazadeh, M. Yakhchalian, Probabilistic residual drift assessment of SMRFs with linear and nonlinear viscous dampers, J. Constr. Steel Res. 148 (2018) 409–421, https://doi.org/10.1016/j.jcsr.2018.05.031.
[42] Eurocode 8, Design of Structures for Earthquake Resistance, vol. 3, 2009. EN 1998.
[43] J. Hancock, J.J. Bommer, Using spectral matched records to explore the influence of strong-motion duration on inelastic structural response, Soil Dynam. Earthq. Eng. 27 (2007) 291–299, https://doi.org/10.1016/j.soildyn.2006.09.004.
[44] J. Hancock, J.J. Bommer, P.J. Stafford, Numbers of scaled and matched accelerograms required for inelastic dynamic analyses, Earthq. Eng. Struct. Dynam. (2008) 1585–1607, https://doi.org/10.1002/eqe.827.
[45] L. Alatik, N. Abrahamson, An improved method for nonstationary spectral matching, Earthq. Spectra 26 (2010) 601–617, https://doi.org/10.1193/1.3459159.
[46] Seismosoft, Seismomatch - a Computer Program for Spectrum Matching of Earthquake Records, 2023.
[47] F. Cedrón, A.Y. Elghazouli, Assessment and design considerations for single layer cylindrical lattice shells subjected to seismic loading, Structures 31 (2021) 940–960, https://doi.org/10.1016/j.istruc.2021.02.023.
[48] W. Hare, J. Nutini, S. Tesfamariam, A survey of non-gradient optimization methods in structural engineering, Adv. Eng. Software 59 (2013) 19–28, https://doi.org/10.1016/j.advengsoft.2013.03.001.
[49] J.H. Holland, Adaptation in natural and artificial systems: an introductory analysis with applications to biology. Control, and Artificial Intelligence, MIT press, 1992.
[50] F.-A. Fortin, F-M De Rainville, M.-A. Gardner, M. Parizeau, C. Gagné, DEAP: evolutionary algorithms made easy, J. Mach. Learn. Res. 13 (2012) 2171–2175.